

Phosphorylation of the smooth muscle master splicing regulator RBPMS regulates its splicing activity

Michael D. Barnhart¹, Yi Yang^{1,†}, Erick E. Nakagaki-Silva^{1,†}, Thomas H. Hammond¹, Mariavittoria Pizzinga², Clare Gooding¹, Katherine Stott¹ and Christopher W.J. Smith^{1,*}

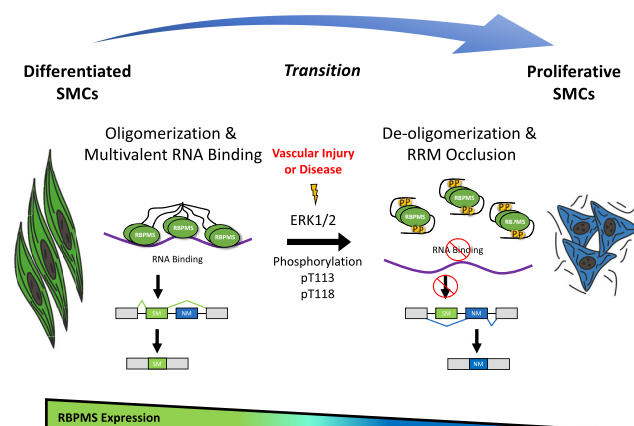
¹Department of Biochemistry, University of Cambridge, Cambridge CB2 1QW, UK and ²MRC Toxicology Unit, University of Cambridge, Cambridge CB2 1QR, UK

Received August 11, 2022; Revised October 12, 2022; Editorial Decision October 12, 2022; Accepted October 24, 2022

ABSTRACT

We previously identified RBPMS as a master regulator of alternative splicing in differentiated smooth muscle cells (SMCs). RBPMS is transcriptionally downregulated during SMC dedifferentiation, but we hypothesized that RBPMS protein activity might be acutely downregulated by post-translational modifications. Publicly available phosphoproteomic datasets reveal that Thr113 and Thr118 immediately adjacent to the RRM domain are commonly both phosphorylated. An RBPMS T113/118 phosphomimetic T/E mutant showed decreased splicing regulatory activity both in transfected cells and in a cell-free *in vitro* assay, while a non-phosphorylatable T/A mutant retained full activity. Loss of splicing activity was associated with a modest reduction in RNA affinity but significantly reduced RNA binding in nuclear extract. A lower degree of oligomerization of the T/E mutant might cause lower avidity of multivalent RNA binding. However, NMR analysis also revealed that the T113/118E peptide acts as an RNA mimic which can loop back and antagonize RNA-binding by the RRM domain. Finally, we identified ERK2 as the most likely kinase responsible for phosphorylation at Thr113 and Thr118. Collectively, our data identify a potential mechanism for rapid modulation of the SMC splicing program in response to external signals during the vascular injury response and atherogenesis.

GRAPHICAL ABSTRACT



INTRODUCTION

Noncommunicable diseases (NCDs), specifically cardiovascular diseases (CVDs), are the leading cause of global death rates. Of the 56.9 million global deaths in 2016, 40.5 million were due to NCDs, of which the leading cause of NCDs was CVD totaling 17.9 million, with >75% of these deaths occurring in low- and middle-income countries (1, <https://www.who.int/news-room/fact-sheets/detail/noncommunicable-diseases>). Pathological blood vessel narrowing carries the highest mortality rate of all the CVDs as a result of the dysregulation of vascular smooth muscle cells (VSMCs), a response that cannot yet be therapeutically controlled. Thus, novel therapeutics and early diagnostic methods at low costs are imperative to reduce the economic burden these diseases carry (2) and it is vital to develop a deeper understanding of CVD mechanisms, par-

*To whom correspondence should be addressed. Tel: +44 1223 333655; Email: cwjs1@cam.ac.uk

†The authors wish it to be known that, in their opinion, the second and third authors should be regarded as Joint Second Authors.

Present addresses:

Erick E. Nakagaki-Silva, Cold Spring Harbor Laboratory, Cold Spring Harbor, NY 11724, USA.

Thomas H. Hammond, Francis Crick Institute, London NW1 1AT, UK.

Mariavittoria Pizzinga, Structural Biology Research Centre, Fondazione Human Technopole, Milan 20157, Italy.

ticularly the molecular mechanisms underlying the control of VSMCs.

Dysfunctional VSMCs drive several CVDs such as atherosclerosis and restenosis, cerebral microangiopathy, Marfan syndrome, hypertension and pulmonary arterial hypertension (2). Coronary artery diseases (CADs), atherosclerosis and restenosis, are the most common CVDs and thus the major cause of death worldwide. During atherosclerosis and restenosis, VSMCs are stimulated to proliferate by platelet-derived growth factor (PDGF) driving the infiltration and migration of VSMCs to the intima and resulting in the progressive thickening and narrowing of the blood vessel lumen (3), ultimately leading to ischemic heart disease and stroke. In fact, VSMC phenotypic dysregulation is the underlying cause of each of the aforementioned diseases. Therefore, understanding this VSMC phenotypic switch from quiescent-contractile to migratory-proliferative on the molecular level is critical and must be pursued. While the transcriptional program underpinning VSMC phenotypic switching has been well studied, the accompanying program of regulated alternative splicing (AS), and the RNA-binding proteins (RBPs) responsible for regulating it, are less well characterized.

To this end, RBPMS (RNA Binding Protein with Multiple Splicing) was recently identified as a potential SMC master splicing regulator, responsible for controlling numerous components critical to differentiated VSMC function (4). RBPMS was found to be highly expressed in the differentiated phenotype and not detected in the dedifferentiated (proliferative) phenotype, suggesting a regulatory role in differentiated SMCs (4). In differentiated SMCs, RBPMS was found to both repress exons included within the dedifferentiated phenotype by binding upstream or within the repressed exons (found in transcripts such as *ACTN1* and *TPM1*) and activate the inclusion of exons found in the differentiated phenotype by binding downstream of the included exon (found in transcripts such as *FLNB*, *MPRIIP* and *PTPRF*) (4). RBPMS has a single RRM domain that mediates both RNA binding to CAC motifs as well as dimerization followed by an intrinsically disordered C-terminal tail of 84 amino acids in the canonical RBPMS-A isoform (Figure 1A). The reported binding motif of RBPMS consists of tandem CACs with a variable spacer of ~1–12 nucleotides, consistent with the dimeric structure (5,6). The canonical isoform, RBPMS-A, was found to be more active in overall splicing regulation compared to the other isoforms; in particular, RBPMS-A could both repress and activate target exons while RBPMS-B was only able to activate (data not shown).

Upon knockdown of RBPMS in differentiated PAC1 cells (a well-established SM cell line), alterations of alternative splicing in numerous genes encoding components of the actin cytoskeleton and cell adhesion machinery were accompanied by reorganization of actin structures to resemble the dedifferentiated phenotype (4). Moreover, overexpression of RBPMS in PAC1 cells was able to recapitulate some differentiated SMC AS patterns that are usually only observed in fully differentiated tissue SMCs, but not in cell culture. Moreover, the SMC transcription factor Myocardin was recently shown to drive the SMC AS program in part by up-regulating RBPMS transcription (7).

These findings demonstrate that RBPMS is a master regulator of the alternative splicing program found in differentiated smooth muscle cells. Thus, the maintenance of the differentiated state is controlled by both transcriptional regulation and alternative splicing regulation (4). Therefore, the precise control of this splicing regulator is vital in determining SMC fate. RBPMS was identified as a candidate master regulator based on the super-enhancer associated with the *RBPMS* gene in SMC-rich tissues, and it is transcriptionally down-regulated in phenotypic modulation (4). However, transcriptional down-regulation does not provide for rapid down-regulation of the activity of proteins already present in the cell.

Various growth factors activate the dedifferentiation of VSMCs by initiating the classical Ras/Raf/MEK/ERK pathway which leads to the downstream phosphorylation of several different families of proteins (2). Phosphorylation of RNA-binding proteins (RBPs), specifically splicing regulators, has been shown to affect proteins in different ways including, but not limited to, protein function, localization, and degradation (8–11). We were thus interested in the possibility that upon the onset of phenotypic transition, phosphorylation might play a role in the acute regulation of RBPMS protein activity. Therefore, we set out to determine if RBPMS could be phosphorylated and, if so, what role this plays in modulating its activity. We found that ERK2 phosphorylates RBPMS-A at Thr113, Thr118, just downstream of the RRM domain (Figure 1A), and Ser144, dependent on a downstream F-site. The use of phosphomimetic mutants indicated that phosphorylation of Thr113 and Thr118, but not Ser144, results in the inhibition of RBPMS-A splicing activity which leads to a splicing profile found in proliferative SMCs. Furthermore, phosphorylation of Thr113 and Thr118 leads to reduced RNA-binding due to both a reduction in oligomerization and associated avidity of multivalent RNA interaction as well as a direct occlusion of the RNA-binding surface of the RRM domain, as elucidated via biochemical assays and NMR. Overall, our data provide a molecular basis for the rapid modulation of RBPMS-A activity by phosphorylation in response to external signals during the vascular injury response and atherogenesis.

MATERIALS AND METHODS

Growth conditions for bacterial cultures

Escherichia coli grown on lysogeny broth (LB) agar was incubated overnight at 37°C, while *E. coli* grown in LB liquid media was incubated at 37°C overnight (or for a minimum of 8 h) and agitated at 280 RPM. Both media contained the appropriate antibiotic; the final concentration of ampicillin used was 50 µg/ml, while kanamycin was 30 µg/ml. For small-scale (miniprep) DNA purification, 5 ml of LB was used, while large-scale (maxiprep) required 100 ml.

Transformation of *E. coli*

Laboratory stocks of chemically competent *E. coli* cells (TG-1) stored at –80°C were used for bacterial transformation via heat shock. 100 µl of TG-1 cells were added and mixed with 100 ng of plasmid DNA or 2.5 µl of a ligation reaction (see below) and incubated on ice for 30 min. The mix

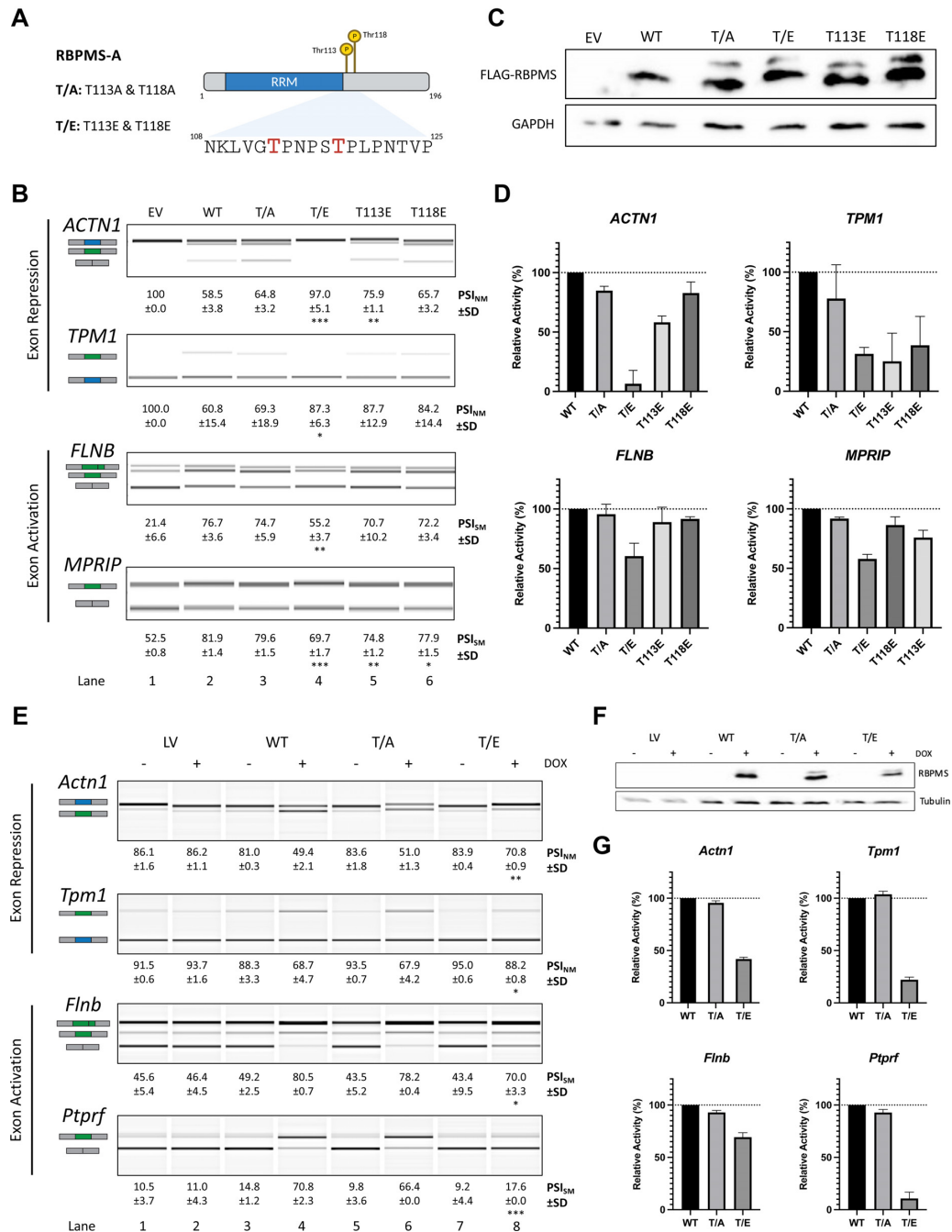


Figure 1. RBPMS-A phosphomimetics have reduced splicing activity across cell lines. (A) Graphical representation of RBPMS-A with the T113 and T118 highlighted in red. T/A is a double mutant of T113A and T118A, while T/E is double mutant of T113E and T118E. Created with BioRender.com. (B) Splicing analysis of the exon repression function of wild-type (WT) RBPMS-A and effectors in endogenous *ACTN1* and *TPM1*, and its exon activation function in endogenous *FLNB* and *MPRIP* in HEK293T cells. RT-PCR followed by visualization on QIAxcel. Cartoons below the gene names represent the PCR products. The blue exon in the cartoon represents the NM (non-smooth muscle) exon, while the green exon represents the SM (smooth muscle) exon. PSI (percent spliced in) values are the mean \pm SD ($n = 3$). A Student's t -test was used to determine statistical significance between wild-type RBPMS-A and effector. EV = empty vector. (C) Immunoblot of FLAG-RBPMS effectors used for splicing assays in (B). Whole-cell lysates were probed with antibodies to FLAG and GAPDH. GAPDH was used as a loading control. (D) Bar graphs showing the percent relative splicing efficiency of each effector normalized to wild-type RBPMS-A (black bar) after background splicing was taken into consideration. (E) Splicing analysis of the exon repression function of wild-type (WT) RBPMS-A and effectors in endogenous *Actn1* and *Tpm1*, and its exon activation function in endogenous *Flnb* and *Ptpf* in rat PAC1 cells. RT-PCR followed by visualization on QIAxcel. Cartoons below the gene names represent the PCR products. The blue exon in the cartoon represents the NM (Non-smooth Muscle) exon, while the green exon represents the SM (smooth muscle) exon. PSI (percent spliced in) values are the mean \pm SD ($n = 3$). A Student's t -test was used to determine statistical significance between wild-type RBPMS-A and effector. LV = empty lentiviral vector. (F) Immunoblot of Dox inducible RBPMS effectors used for splicing assays in (E). Whole-cell lysates were probed with antibodies to RBPMS and tubulin. Tubulin was used as a loading control. (G) Bar graphs showing the percent relative splicing efficiency of each effector normalized to wild-type RBPMS-A (black bar), after background splicing was taken into consideration. Error bars indicate SD. Significance in panels (B) and (E) indicated by * $P < 0.05$, ** $P < 0.01$, *** $P < 0.001$.

was then heat shocked at 42°C for 30 s and then placed back on ice for five minutes. Finally, the entire mix was spread on LB agar plates containing the appropriate antibiotic and incubated as described above.

Ligation of DNA fragments

Ligation reactions were set up in a 1:3 ratio of vector:insert, calculated from base-pair length. T4 DNA ligase (Roche) was used, and the final reaction volume was 10 μ l. Ligation reactions were then used for *E. coli* transformations as described above.

Plasmid DNA purification

Following transformation, single colonies of *E. coli* were picked from the LB agar plates and placed in either 5 ml LB for miniprep or 100 ml for maxiprep with the appropriate antibiotic. Cultures were incubated at 37°C, agitating at 280 RMP, for at least 8 hours for minipreps and overnight for maxipreps. Bacterial cells were then pelleted at either 4800 \times g for 5 min for minipreps and 5000 \times g for 15 mins for maxipreps at 4°C. Manufacturer's instructions for the QIAGEN QIAprep Spin Miniprep or Maxiprep kits were then followed for cell lysis and plasmid DNA purification. A NanoDrop spectrometer (Thermo Scientific) was used to measure the final purified plasmid DNA concentration and appropriate dilutions were made with ddH₂O and stored at -20°C.

Purification of DNA fragments

DNA fragments that were amplified by PCR were purified using a QIAGEN QIAquick PCR Purification Kit. If restriction digestion was necessary, the DNA fragment was run on an agarose gel and then excised and purified using a QIAGEN QIAquick Gel Extraction Kit. DNA fragments were eluted with ddH₂O and stored at -20°C.

DNA construct generation

RBPMS-A constructs (wild-type and some mutant) were previously generated in the lab and cloned into pEGFP-C1. However, to reduce the size of the N-terminal tag, all constructs were cloned into either pCI-3xFLAG at *EcoRI* and *BamHI* or pCI-3xFLAG-NLS at *XhoI* and *BamHI* for use *in vivo* overexpression in HEK293T cells. An exogenous nuclear localization signal (NLS) was used to ensure the nuclear localization of the deletion mutants, given that RBPMS NLS is not well characterized.

Oligonucleotides for the desired mutagenesis of RBPMS were designed using the Agilent QuikChange Primer Design software available online followed by mutagenesis PCR according to the manufacturer's guidelines. Deletion mutants were generated by designing oligonucleotide primers that amplified in the opposite direction, leaving the desired deletion omitted from amplification. The blunt ends that were generated were then phosphorylated and ligated. Parental plasmids in both mutant and deletion generation were digested using *DpnI* enzyme.

RBPMS-A and various mutants were subcloned into a modified pET15b-TEV vector (Yi Yang *et al.*, in preparation) at *Sall* and *XhoI* for the expression of recombinant protein in *E. coli*. The pET15b vector was modified by replacing the thrombin site with a TEV site and replacing the *NdeI* site with *SlaI* because both sites are present in RBPMS-A.

MEK1, CA-MEK1, and ERK2 were subcloned from pIVEX_MEK1 (WT), pET28a_MEK1_del44-51_S218D_M219D_N221D_S222D (Highly Constitutively Active), and pET28a_ERK2 (WT), respectively, and cloned into pCI-3xFLAG at *AvrII* and *XhoI*. These constructs were obtained from Remkes Scheele, Department of Biochemistry, University of Cambridge.

The sequences of each construct were verified by Sanger sequencing. The oligonucleotides used to create each construct can be found in Table 1.

Cell culture

The rat pulmonary artery cell (PAC1) line was used in this study because they are a well-established smooth muscle cell model (12). Additionally, the human embryonic kidney cell line with a mutated version of the SV40 large T antigen (HEK 293T) was used as an alternative cell line due to the poor transfection efficiency of PAC1 cells.

Both cell lines were cultured in Dulbecco's Modified Eagle Medium (DMEM, Gibco) containing 1% glutamax and 10% fetal bovine serum (FBS). Cells were cultured under standard conditions, 37°C and 5% CO₂. HEK293T cells were passaged twice a week at a 1:15 dilution, while PAC1 cells were only passaged once a week at a 1:10 dilution to maintain the differentiated state and avoid stimulating them to become more proliferative.

Transient transfections

HEK293T cells were seeded in a six-well plate at a concentration of 2×10^5 cells/well at least 8 hours prior to transfection. For each well, 2 μ l of Lipofectamine 2000 reagent (Thermo Fisher) and 1 μ g of DNA were diluted in OptiMEM (Gibco). Cells were incubated under standard conditions (described above) for 48 h at which time total RNA and protein were harvested.

Inducible lentiviral overexpression

The inducible lentiviral overexpression cell lines used in this study were created using pInducer22 plasmids and the Gateway System (13). Overexpression was achieved by inducing the cells with 1 μ g/ml of doxycycline diluted in the cell culture medium. Total RNA and protein were harvested 24 h post-induction.

Western blotting

Western blotting was used to verify the protein expression levels of the overexpression experiments. Total lysates were harvested by the direct addition of 1xSDS + 5% β -mercaptoethanol and stored at -80°C. Lysates were then boiled at 95°C, run on an SDS-PAGE gel, and transferred

Table 1. Oligonucleotide sequences used for the generation of DNA constructs

Construct	5'-3' Oligonucleotide sequence	Vector	Cloning method	Experiment
RBPM5-A WT	CCGGAATTCACGGCGGGCA CGCGATCCTTAGCAGAACTGCCGGACTTC	pCI-3xFLAG	<i>EcoRI</i> - <i>BamHI</i>	<i>in vivo</i> OE
RBPM5-A T/E	CCGGAATTCACGGCGGGCA CGCGATCCTTAGCAGAACTGCCGGACTTC	pCI-3xFLAG	<i>EcoRI</i> - <i>BamHI</i>	<i>in vivo</i> OE
RBPM5-A T/A	CCGGAATTCACGGCGGGCA CGCGATCCTTAGCAGAACTGCCGGACTTC	pCI-3xFLAG	<i>EcoRI</i> - <i>BamHI</i>	<i>in vivo</i> OE
RBPM5-A T113E	CCGGAATTCACGGCGGGCA CGCGATCCTTAGCAGAACTGCCGGACTTC	pCI-3xFLAG	<i>EcoRI</i> - <i>BamHI</i>	<i>in vivo</i> OE
RBPM5-A T118E	CCGGAATTCACGGCGGGCA CGCGATCCTTAGCAGAACTGCCGGACTTC	pCI-3xFLAG	<i>EcoRI</i> - <i>BamHI</i>	<i>in vivo</i> OE
RBPM5-A S117E	AGTGTGGCAGAGAGTCTCGGGTTGGAGTCCCTAC GTAGGGACTCCAAACCCGAGACTCCTCTGCCCAACACT	pCI-3xFLAG	<i>Mutagenesis</i>	<i>in vivo</i> OE
RBPM5-A WT + NLS	CGGCTCGAAGACGGCGGGCA CGCGATCCTTAGCAGAACTGCCGGACTTC	pCI-3xFLAG-NLS	<i>XhoI</i> - <i>BamHI</i>	<i>in vivo</i> OE
RBPM5-A T/E + NLS	CGGCTCGAAGACGGCGGGCA CGCGATCCTTAGCAGAACTGCCGGACTTC	pCI-3xFLAG-NLS	<i>XhoI</i> - <i>BamHI</i>	<i>in vivo</i> OE
RBPM5-A T/A + NLS	CGGCTCGAAGACGGCGGGCA CGCGATCCTTAGCAGAACTGCCGGACTTC	pCI-3xFLAG-NLS	<i>XhoI</i> - <i>BamHI</i>	<i>in vivo</i> OE
RBPM5-A WT	ACGGCTGACACGGCGGGCA CCGCTCGAGTTATTAGCAAACTGCCGGGACTTC	pET-15b	<i>Sall</i> - <i>XhoI</i>	Recombinant protein
RBPM5-A T/E	ACGGCTGACACGGCGGGCA CCGCTCGAGTTATTAGCAAACTGCCGGGACTTC	pET-15b	<i>Sall</i> - <i>XhoI</i>	Recombinant protein
RBPM5-A T/A	ACGGCTGACACGGCGGGCA CCGCTCGAGTTATTAGCAAACTGCCGGGACTTC	pET-15b	<i>Sall</i> - <i>XhoI</i>	Recombinant protein
RBPM5-A Δ112-119	CTGCCAACACTGTACCTC TACGAGTTTCTTGGCCATC	pCI-3xFLAG-NLS	<i>Deletion</i>	<i>in vivo</i> OE
RBPM5-A S144A	CACACTCAGGGCACTGGGTAAAGTGCAGGTACTG CAGTACCTGCACCTTACCCAGTCCCTGAAGTGTG	pCI-3xFLAG	<i>Mutagenesis</i>	<i>in vivo</i> OE
RBPM5-A S144E	GGGCCACACTCAGGTTCAGTGGGTAAAGTGCAGGTACT GTACCTGCACCTTACCCAGTGAACCTGAAGTGTGGGCC	pCI-3xFLAG	<i>Mutagenesis</i>	<i>in vivo</i> OE
RBPM5-A ΔF-Site	GCTTCACTGCATGCCAG AGCGGACGAGGAGGAAAG	pCI-3xFLAG	<i>Deletion</i>	<i>in vivo</i> OE
RBPM5-A T12A	GCCTCGCTCGGGGCTTCTCCTCTCG CGAGAAGGAGAACGCCCGAGCGAGGC	pCI-3xFLAG	<i>Mutagenesis</i>	<i>in vivo</i> OE
RBPM5-A T12E	GGTTGGCTCGCTCGTTCCTCTCCTCTCGGCT AGCCGAGAAGGAGAACGCCAGCGAGCGAGGCCAAC	pCI-3xFLAG	<i>Mutagenesis</i>	<i>in vivo</i> OE
MEK1 WT	CCGCTCAGTCACTAACTAGTGTAGGCTTGCA CCGCTAGGATGCCCAAGAAGACCC	pCI-3xFLAG	<i>AvrII</i> - <i>XhoI</i>	<i>in vivo</i> OE
CA-MEK1	CCGCTCAGTCACTAACTAGTGTAGGCTTGCA CCGCTAGGATGCCCAAGAAGACCC	pCI-3xFLAG	<i>AvrII</i> - <i>XhoI</i>	<i>in vivo</i> OE
ERK2	TATCCTAGGATGCCGGCGGG CCGCTCAGTCACTAACTAGTGTATCCTCGCTGG	pCI-3xFLAG	<i>AvrII</i> - <i>XhoI</i>	<i>in vivo</i> OE
RBPM5-A WT NMR	ACGGCTGACACGGCGGGCA CCGCTCAGTTCAGTGTGGCAGAGGAGTACTG	pET-15b	<i>Sall</i> - <i>XhoI</i>	Recombinant protein
RBPM5-A T/E NMR	ACGGCTGACACGGCGGGCA CCGCTCAGTTCAGTGTGGCAGAGGAGTACTG	pET-15b	<i>Sall</i> - <i>XhoI</i>	Recombinant protein

Table 2. Antibodies used in this study for western blotting

Protein	Antibody	Concentration
FLAG	Sigma Aldrich, F-1804	1:2000
GAPDH	Santa Cruz, sc-47724	1:1000

to an Immobilon-FL membrane (Millipore). Specific proteins were detected by the primary antibodies listed in Table 2. Donkey anti-mouse IgG antibodies (Strattech Scientifica) conjugated to horseradish peroxidase were used at a 1:10 000 dilution. Antibody detection was carried out using luminol/iodophenol chemiluminescence followed by imaging on a Bio-Rad ChemiDoc and analysis on Image Lab (v6.0).

Immunofluorescence

HEK293T cells were seeded on a Corning BioCoat Poly-D-Lysine 8-well culture slide at a concentration of 14×10^3 cells/well at least 8 h prior to transfection. Forty-eight hours post-transfection, slides were incubated in 3.8% paraformaldehyde (PFA) for 5 min then rinsed with phosphate-buffered saline (PBS). Cells were then permeabilized with 0.5% NP-40 for 2 min and rinsed with PBS. 1% bovine serum albumin (BSA) in PBS (blocking buffer) was used to block the cells for 1 h and replaced with anti-FLAG antibodies (Sigma Aldrich, F-1804) diluted in blocking buffer (1:1000) for an additional hour. Next, cells were rinsed with PBS and incubated with anti-mouse Rhodamine Red-X (Thermo Fisher, R-6393) diluted in blocking buffer (1:500) for 1 h. Following a final rinse with PBS, the chambers were detached from the slides, and coverslips were mounted using ProLong Diamond Antifade with DAPI (Thermo Fisher). All incubations were carried out at room temperature. Images were acquired on a Zeiss Axio Observer.Z1 LSM 980 microscope equipped with Airyscan 2, using ZEN Blue software (version 3.3), in Airyscan super-resolution imaging mode. A C-Apochromat 40X /1.20 W Korr objective was used. 15/20 Z-slices per image were acquired at an interval of 0.2 μm . Airyscan processing with standard parameters was applied to each image in Zen Blue software. Further processing and analysis were performed using Fiji software (version 2.3.051). Supplementary data images of cells were visualized and acquired using an EVOS M5000 with a 40 \times objective and analyzed on EVOS M5000 software (v1.3).

RT-PCR

TRI reagent (Sigma) was used to extract total RNA from cells following the manufacturer's guidelines. Genomic DNA was then degraded using Turbo DNase (Thermo Fisher) and RNA was quantified on a NanoDrop spectrometer (Thermo Fisher). 1 μg of total RNA along with oligo dTs and SuperScriptII (Thermo Fisher) were used to prepare cDNA following the manufacturer's protocol.

Alternative splicing analysis

To detect changes in splicing isoforms, PCR reactions were prepared with 1 μl of cDNAs (described above), oligonu-

cleotides targeting specific genes (Table 3), and Jumpstart Taq DNA polymerase (Sigma). The following PCR parameters were used: initial denaturation at 94°C for 3 min; 35 cycles of 94°C for 30 s, 60°C for 30 s and 72°C for 60 s; final elongation at 94°C for 30 s. Reaction was then slow cooled, $\Delta T - 1^\circ\text{C}$ every min down to 37°C.

QIAxcel Advanced System (QIAGEN) was used to separate the PCR products and QIAxcel ScreenGel software was used to analyze the PCR products and calculate the percentage spliced in (PSI) value. PSIs are shown as the mean (%) \pm standard deviation of at least three experiments. Negative controls included a no template (cDNA) reaction and minus RT reaction.

Recombinant protein expression

RBPMS-A wild-type and mutants were cloned into modified pET15b vectors containing an N-terminal His₆ tag and a TEV protease site. BL21 competent cells were then transformed with each construct and a single colony was then inoculated in 10 ml of LB + ampicillin (50 $\mu\text{g}/\text{ml}$) and grown for 12 h at 37°C, 280 RPM. This cell slurry was then added to 500 ml of LB + ampicillin (50 $\mu\text{g}/\text{ml}$) and incubated at 37°C, 220 RPM for ~ 2 h until the OD reached 0.6–0.8 (log phase growth). 0.2 mM of IPTG (isopropyl β -D-1-thiogalactopyranoside) was added to induce the expression of protein for 2 h at 37°C, 220 RPM. Cells were then pelleted at 7000 $\times g$ for 10 min at 4°C and resuspended in 10 ml of Buffer A (50 mM Tris base, 0.5 M KCl, 40 mM imidazole, 10% glycerol, pH 8.5 at 4°C). 1 mM DTT, 1.6 M LiCl and 2 cComplete™ mini protease inhibitor cocktail (Roche) tablets were added to the cell suspension followed by cell lysis using a French Press (Stansted). Lysates were centrifuged at 40 000 $\times g$ for 30 min at 4°C for the separation of soluble and insoluble fractions. Soluble fractions were filtered using a 0.45 μm filter in preparation of protein purification.

Purification of RBPMS

Filtered soluble recombinant wild-type RBPMS-A and mutants were purified on an AKTA protein purification system (GE Healthcare). Recombinant protein was first purified on HisTrap HP column (GE Healthcare) using Buffer A (50 mM Tris Base, 0.5 M KCl, 40 mM imidazole, 10% glycerol, 1 mM DTT, pH 8.5 at 4°C), Buffer A2 (50 mM Tris base, 2 M NaCl, 10% glycerol, 1 mM DTT, pH 8.5 at 4°C), and Buffer B (50 mM Tris base, 0.5 M KCl, 500 mM imidazole, 10% glycerol, 1 mM DTT, pH 8.5 at 4°C). After fraction analysis on SDS-PAGE, the fractions containing recombinant protein were buffer exchanged to Buffer QA (25 mM CAPS, 50 mM KCl, 10% glycerol, pH 10 at 4°C) followed by TEV protease cleavage at a ratio of 1:40 for 2 h at 30°C and stored overnight at 4°C. Cleaved recombinant protein was then purified on a MonoQ 5/50 GL column (GE Healthcare) using Buffer QA (described above + 1 mM DTT) and Buffer QB (25 mM CAPS, 50 mM KCl, 1 M NaCl, 10% glycerol, 1 mM DTT, pH 10 at 4°C). Fractions with pure protein, as analyzed by SDS-PAGE (Supplementary Figure S6), were pooled, quantified on a NanoDrop spectrometer (Thermo Scientific), concentrations determined using predicted extinction coefficients, and stored at -80°C .

Table 3. Oligonucleotide sequences used to study alternative splicing

Gene	Genome	Regulated exon	5'-3' Sequence
<i>FLNB</i>	hg19	Chr3:58127584–58127623(+)	ATCGCCTCCACTGTGAAAAC AATCCCAGGCCGTTTCATGTC
<i>MPRIIP</i>	hg19	Chr17:17083920–17083983(+)	ACCCGGCAACTCAGAAAACATC AGCTTCAACCGTTCTTGCAC
<i>TPM1</i>	hg19	Chr15:63335905–63336030(+)	GAGCTGGCAGAGAAAAAAG AGGAGGACATCGCGGCCA TCCAACCTCTCCTCAACCAG
<i>ACTN1</i>	hg19	Chr14:69345705–69345786(–)	CAGATCCTGACCCGGGATG CATGACTTGGTCTGCTGTATCTGT
<i>Tpm1</i>	rn6	Chr8:72840038–72840164(–)	AGGAGGACATCTCAGCAA GAGCTGGCGGAGAAAAAAG TCCAACCTCCTCAACCAG
<i>Actn1</i>	rn6	Chr6:103379819–103379900(–)	CAGATCCTGACCCGGGATG CATGACTTGGTCTGCTGTATCTGT
<i>Ptprf</i>	rn6	Chr5:137046364–137046397(–)	CGTCAAAGGATGAGCAGTCAATC CCCATCATTGGCTTTGAGAC
<i>Flnb</i>	rn6	Chr15:18780269–18780341(–)	CAGGGAAGGGGAAAAGTCACC ACTCACTGGGACATAGGCCCT

In vitro transcription

RNA transcripts for *in vitro* splicing, EMSAs, and UV-crosslinking were transcribed from pGEM vectors with T7 RNA polymerase as described previously (4,14–15), albeit to aid in visualization, [α - 32 P]CTP was used to label the RNAs instead of [α - 32 P]UTP.

For high yield RNA transcripts for splicing assays and EMSAs, the reaction contained 1 μ g of linearized DNA, 2 μ l of 5 \times transcription buffer (30 mM MgCl₂, 10 mM spermidine, 0.2 M Tris-HCl, pH 7.5), 1 μ l 10 \times rNTPs (5 mM UTP, 5 mM ATP, 5 mM GTP, 2 mM CTP), 0.5 μ l RNasin (Promega), 0.5 μ l 10 mM RNA cap analogue (Promega), 2.5 μ l ddH₂O, 1.5 μ l T7 RNA polymerase and 1 μ l of 0.37 MBq/ μ l [α - 32 P]CTP. The transcripts for UV-crosslinking required high specific activity and the reactions were adjusted to 0.4 mM CTP and 2 μ l of 0.37 MBq/ μ l [α - 32 P]CTP. Reactions were incubated for 2 h at 37°C followed by a 1:5 dilution with ddH₂O and 1 μ l was taken for total scintillation counts. RNAs were then phenol extracted and spun in a G-50 column (ProbeQuant) at 3000 \times g for 2 min to purify the RNAs. A Beckman LS 3801 scintillation counter was used to quantify the radioactivity of 1 μ l of purified RNAs along with the 1 μ l total sample. The percentage yield was calculated by dividing the [incorporated RNA counts \times final volume] by [total RNA counts \times 50 μ l]. The [percent yield/100] \times [mass of the nucleotide \times number of nucleotides \times CTP concentration \times volume] was used to calculate the amount of RNA transcribed. The transcribed RNAs were then diluted to 20 fmol/ μ l with ddH₂O.

The transcripts used in the splicing assays contained α -tropomyosin exons 1, 3 and 4 and the introns between exons 1–3 and 3–4 (known as TM1-3-4) providing a sufficient pre-mRNA transcript to analyze splicing activity. The transcripts used in the UV-crosslinking assays were a truncated version of TM1-3-4, containing only the exon 3 and flanking introns. While the transcript used in the EMSAs was a synthetic RNA of 120 nucleotides containing three tandem CAC motifs modeled after the intronic region between exons 1 and 3 of TM1-3-4 (Yi Yang *et al.*, in preparation).

In vitro splicing assay

Splicing reactions contained 10 μ l total volume: 2.6% polyvinyl alcohol, 2 mM MgCl₂, 500 μ M ATP, 20 mM creatine phosphate, 300 U/ μ l RNasin (Promega), 12 mM HEPES, pH 7.9, 0.3 mM DTT, 30% HeLa nuclear extract and 12.5 ng α - 32 P labelled pre-mRNA. Reactions were incubated at 30°C for 3 h, subjected to proteinase K digestion, phenol extracted, and ethanol precipitated. Reaction products were finally resolved on an 8 M urea–4% polyacrylamide gel. Gels were then dried and visualized by autoradiography on a GE Typhoon FLA 9000. Nuclear extracts were prepared from HeLa cells in suspension using the modifications described previously (16).

Electrophoretic mobility shift assay

Wild-type recombinant RBPMS-A or the mutant variants were titrated (4, 2, 0.66, 0.22, 0.07, 0.024, 0 μ M) and incubated with 20 fmol of *in vitro* transcribed RNA in binding buffer (50 mM HEPES pH 7.2–7.9, 15 mM MgCl₂, 25% glycerol, 5 mM DTT, 45 mM KCl, 5 μ g tRNA) for 25 min at 30°C. Heparin (5 μ g) was then added to remove non-specific binding and incubated for an additional 5 min at 30°C. 1 μ l of 50% glycerol was added to the reactions before loading onto a 4% 60:1 acrylamide:bisacrylamide non-denaturing gel with TBE running buffer at room temperature. Gels were then dried and visualized by autoradiography on a GE Typhoon FLA 9000. After phosphor-imaging, the RNA in each lane was quantitated as either 'Free' or 'Bound', where the Bound fraction included complexes of all mobilities, and [bound]/[bound + free] was plotted against total protein concentration. Apparent K_d 's were determined using the Hill equation.

UV-crosslinking

The same binding reaction described above for EMSAs was used for UV-crosslinking, however, 20 fmol of the truncated transcript was used with or without 20% HeLa nuclear extract. Reactions were then UV-crosslinked on ice in

a Stratalinker with two pulses at 960 mJ. An RNase mix (RNase A, 12.5 μg and RNase T1, 0.35 U) was added and the reactions were incubated for 10 min at 37°C. Reactions were quenched by the addition of 4 \times SDS sample buffer, boiled at 80°C for 5 min, and loaded onto a 15% SDS-PAGE gel. Gels were then dried and visualized by autoradiography on a GE Typhoon FLA 9000.

***In vitro* kinase assay**

Kinase assays contained wild-type recombinant RBPMS-A or the non-phosphomimetic T/A mutant and active recombinant ERK2 (obtained from Remkes Scheele, Department of Biochemistry, University of Cambridge). Myelin basic protein (MBP; Millipore) was used as a positive control. Kinase reactions were 30 μl total: 3 μl 10 \times kinase buffer (400 mM Tris-HCl pH 7.5, 100 mM MgCl₂, 1 mM EGTA, 10 mM DTT, 1 \times phosphatase inhibitor), 1 μl kinase (various concentrations), 1 μl substrate (various concentrations), 23 μl ddH₂O, and 2 μl ATP mix (0.5 mM ATP, 0.74 MBq [γ -³²P]ATP (for radiolabeled assays)). Reactions were incubated for 5 min at room temperature and quenched by the addition of 4 \times SDS sample buffer. Samples were separated by 15% SDS-PAGE. Gels were then dried and visualized by autoradiography on a GE Typhoon FLA 9000.

Analytical ultracentrifugation

An Optima XL-I (Beckman Coulter) centrifuge using an An60 Ti eight-hole rotor was used to measure sedimentation velocity (SV). Standard 12 mm double-sector Epon centerpieces with sapphire windows contained 400 μl of wild-type recombinant RBPMS-A or the mutant variants that were buffer exchanged with ultracentrifugation buffer (20 mM HEPES, 500 mM KCl, 1 mM TCEP, pH adjusted to 7.9) and adjusted to 0.5 mg/ml. Interference data were acquired at 40 000 rpm, 20°C, overnight. Ten scans were overlaid as a single point to reduce file size. The partial specific volume of the protein ($\bar{v} = 0.73$ ml/g) and the viscosity and density of the buffer ($\eta = 1.01036 \times 10^{-2}$ mPa-s; $\rho = 1.0232$ g/ml) were calculated using SEDNTERP (Laue *et al.*, 1992). One hundred scans taken over 10 h were used to determine the multi-component sedimentation coefficient $c(s)$ distributions by direct boundary modeling of the Lamm equation using SEDFIT (v14.1) (17). The proportion of dimers to oligomers was determined by integration of the peaks, which were identified by their fitted mass.

Phosphatase assay

Whole-cell extracts of HEK293T cells overexpressing our protein of interest (see transient transfection in methods) were harvested in gentle lysis buffer (150 mM NaCl, 1% Triton X-100, 0.1% SDS, 50 mM Tris pH 8). Extracts (3 μl) were incubated in NEBuffer Pack for Protein MetalloPhosphatases (PMP; 50 mM HEPES, 100 mM NaCl, 2 mM DTT, 0.01% Brij 35, pH 7.5), 10 mM MnCl₂ and 4 U of lambda protein phosphatase for 30 min at 30°C. Protein was then resolved on a 15–20% SDS-PAGE followed by immunoblotting.

NMR spectroscopy

For expression of ¹⁵N- or ¹³C,¹⁵N-labelled RBPMS and mutant proteins, ¹³C₆- glucose and/or ¹⁵NH₄Cl were used as the sole carbon/nitrogen source in M9 minimal medium. NMR measurements were made on ~0.5 mM solutions in 10% ²H₂O, 10 mM HEPES (pH 6.8) and 50 mM KCl. Experiments were recorded on Bruker AVANCE III 600 or 800 MHz spectrometers equipped with QCI or TXI cryoprobes. Experiments were recorded at both 37°C (optimal for the folded regions) and 5°C (optimal for the disordered tails). Established versions (18) of HNCA, HN(CO)CA, HN(CO)CACB, HNCACB, HNCO, 3D TOCSY-¹⁵N-HSQC and NOESY-¹⁵N-HSQC experiments were acquired, alongside HNN (19). Triple resonance experiments were acquired with 25% nonuniform sampling, using Poisson-gap sampling (20), and reconstructed using the Cambridge CS package and the CS-IHT algorithm (21). Data were processed using the AZARA suite of programs (v. 2.8, © 1993–2022; Wayne Boucher and Department of Biochemistry, University of Cambridge, unpublished). Backbone assignments were available for a related protein (BMRB Entry 19298 (22)), which were used as a starting point. Assignment was carried out using CcpNmr Analysis v. 2.4 (23). Chemical-shift differences were calculated using $\Delta\delta = [(\Delta\delta^{\text{H}})^2 + (0.15 \times \Delta\delta^{\text{N}})^2]^{1/2}$ (24).

SEC-MALS

The absolute molecular masses of the truncated RBPMS-A WT and T/E protein samples (used for NMR) were determined by SEC-MALS. 50- μl protein samples (at ~2 mg/ml) were loaded onto a Superdex 75 10/300 GL increase size-exclusion chromatography column (GE Healthcare) in 10 mM HEPES, pH 6.8, 50 mM KCl, at 0.5 ml/min with an ÄKTA Purifier (GE Healthcare). The column output was fed into a DAWN HELEOS II MALS detector (Wyatt Technology) followed by an Optilab T-rEX differential refractometer (Wyatt Technology). Light scattering (LS) and differential refractive index (dRI) data were collected and analyzed with ASTRA 6 software (Wyatt Technology). Molecular masses and estimated errors were calculated across individual eluted peaks by extrapolation from Zimm plots with a dn/dc value of 0.1850 ml g⁻¹. SEC-MALS data are presented with LS and UV plotted alongside fitted molecular masses.

RESULTS

Phosphorylation of RBPMS at Thr113 and Thr118

Post-translation modifications (PTMs) of RBPMS were determined using the PhosphoSitePlus database which collates PTMs of proteins from published datasets (25), filtering for entries from high throughput papers supported by five or more references. Two strongly supported events, phosphorylation of Thr113 and Thr118, occur immediately on the C-terminal side of the RBPMS RRM domain (Figure 1A; Supplementary Figure S1A, original data from refs (26–30)). Not only were these residues and their adjacent prolines phylogenetically conserved (Thr113 across vertebrates, and Thr118 across vertebrates except fish), but

phosphorylation of Thr113 and Thr118 was found in human, rat, and mouse datasets (Supplementary Figure S1B). Moreover, the two phosphorylation events frequently occur together, and in one study were identified in M phase arrested HeLa cells (26,27). Taken together, these data suggest that the possible canonical phosphorylation of RBPMS is at residues T113 and T118, and that phosphorylation of RBPMS could perhaps occur in a cell-cycle-specific fashion.

Phosphomimetic mutations inhibit RBPMS splicing activity in cell culture

Since the most likely phosphorylation of RBPMS occurs on residues Thr113 and Thr118, we made mutations to these residues in the canonical RBPMS-A isoform. We created both non-phosphomimetic and phosphomimetic mutants by mutating both threonine 113 and 118 to either alanine in 'RBPMS-A T/A' or glutamic acid in 'RBPMS-A T/E', as well as the individual mutants, T113E and T118E. Mutants were transiently transfected into HEK293T cells, and their splicing activity was evaluated by assessing their ability to promote SMC AS of endogenous *ACTN1*, *TPM1*, *FLNB*, and *MPRIP* (Figure 1B and D). *ACTN1* and *TPM1* contain non-smooth muscle exons (NM), that are included in the more motile and proliferative phenotype. These exons are repressed by RBPMS-A thereby allowing inclusion of the mutually exclusive smooth muscle (SM) exon. Conversely, *FLNB* and *MPRIP* contain SM cassette exons that are activated by RBPMS-A (4). While WT RBPMS promoted the SMC splicing pattern in each case (Figure 1B, lanes 1 and 2), the phosphomimetic mutant, RBPMS-A T/E, had significantly reduced activity across all transcripts (Figure 1B and D). RBPMS-A T/E significantly failed to repress the NM exons of *ACTN1* and *TPM1* and had significantly impaired activation of the SM exons of *FLNB* and *MPRIP* when compared to wild-type (WT) (Figure 1B, lane 4 versus 2). However, the non-phosphomimetic, RBPMS-A T/A, retained similar repressive and activation activity compared to WT RBPMS-A (Figure 1B, lane 3 versus 2). All proteins were expressed at similar levels (Figure 1C), thus the reduced activity of the phosphomimetic can be directly attributed to the phosphomimetic mutations. The upper bands in Figure 1C represent phosphorylation at S144 (see below). Although the single T113E and T118E mutations showed some reduced splicing activity for some transcripts, neither of them had a significant reduction in activity across all transcripts, which was only observed for the double mutant (Figure 1B and D).

We next set out to determine the effects of the phosphomimetic mutations on RBPMS activity in PAC1 vascular smooth muscle cells. Due to the poor transfection efficiency of plasmids in PAC1 cells, we generated doxycycline-inducible cells using the pInducer22 lentiviral vector (13) to express our RBPMS-A wild-type and mutant constructs. Following a 24-h doxycycline induction, RNA was harvested, and the splicing activity was evaluated by assessing the splice variants of endogenous *Actn1*, *Tpm1*, *Flnb*, and *Ptprf* (Figure 1E and G). As observed in the HEK293T cells, the WT and T/A mutant RBPMS regulated all splic-

ing events (lanes 4 versus 3 and 6 versus 5), but the RBPMS-A T/E mutant failed to repress the NM exons in *Actn1* and *Tpm1* and was significantly impaired for activation of the SM exons in *Flnb* and *Ptprf* (Figure 1E, lane 8 versus 4). Similar expression levels of all RBPMS-A proteins were observed (Figure 1F). Collectively, these data from the HEK293T transfections and now the PAC1 overexpression show that phosphomimetic mutations of RBPMS-A at T113 and T118, and by extension potentially phosphorylation, down-regulates both its exon repression and exon activation splicing activity.

To ensure that the phosphomimetics were not disrupting any regulatory elements that might exist around the area of the mutations, we deleted residues 112 through 119 ($\Delta 112-119$) to capture the region where T113 and T118 reside (Supplementary Figure S1C). This mutant was then transiently transfected into HEK293T cells, and its splicing activity was evaluated by assessing the splice variants of endogenous *ACTN1*, *TPM1*, *FLNB*, and *MPRIP* (Supplementary Figure S1E and F). There was no significant change in splicing activity across all transcripts as the deletion mutant had similar activity to the wild-type protein (Figure 1D). These data suggest that the region containing T113 and T118 is not essential for RBPMS-A activity but acts purely as a site for regulatory input by phosphorylation.

RBPMS-A is a substrate of ERK2

Since the phosphomimetic T/E mutant suggested that the splicing activity of RBPMS-A was down-regulated by its phosphorylation, we wanted to identify the kinase(s) responsible for phosphorylation at T113 and T118. First, we used PhosphoNET Kinase Predictor (www.phosphonet.ca), which determined that the most likely kinase candidate for RBPMS at T113 and T118 was ERK2, with ERK1 identified as the second most likely candidate (Figure 2A). Secondly, we searched current literature for known ERK substrates and found that mouse RBPMS has been shown to be phosphorylated by ERK2 at T118 (31). Mouse RBPMS shares a 98% identity with human RBPMS and is conserved at T113 and T118 (Supplementary Figure S1B). Finally, growth factors, such as PDGF, drive the dedifferentiation of VSMCs by activating the Ras/Raf/MEK/ERK pathway, which could rapidly inactivate the RBPMS-driven splicing program (2).

Given this information, we set out to determine if RBPMS could be phosphorylated by ERK2. A phosphorylation-dependent mobility shift occurs for many eukaryotic proteins in SDS-PAGE (32); therefore, to observe the phosphorylation of RBPMS-A in a cell culture model, we transiently transfected wild-type RBPMS-A along with constitutively active MEK1 (MEK1-CA) and wild-type ERK2 in HEK293T cells and analyzed the protein via western blot. The results showed substantial phosphorylation of RBPMS-A in the presence of MEK1-CA and ERK2 as a large proportion of RBPMS-A had shifted upwards indicating phosphorylation (Figure 2B, lanes 7 versus 5). To confirm *bona fide* phosphorylation of RBPMS-A, we carried out lambda phosphatase treatment prior to western blotting. The collapse back to a single lower RBPMS-A band confirms that the upper band

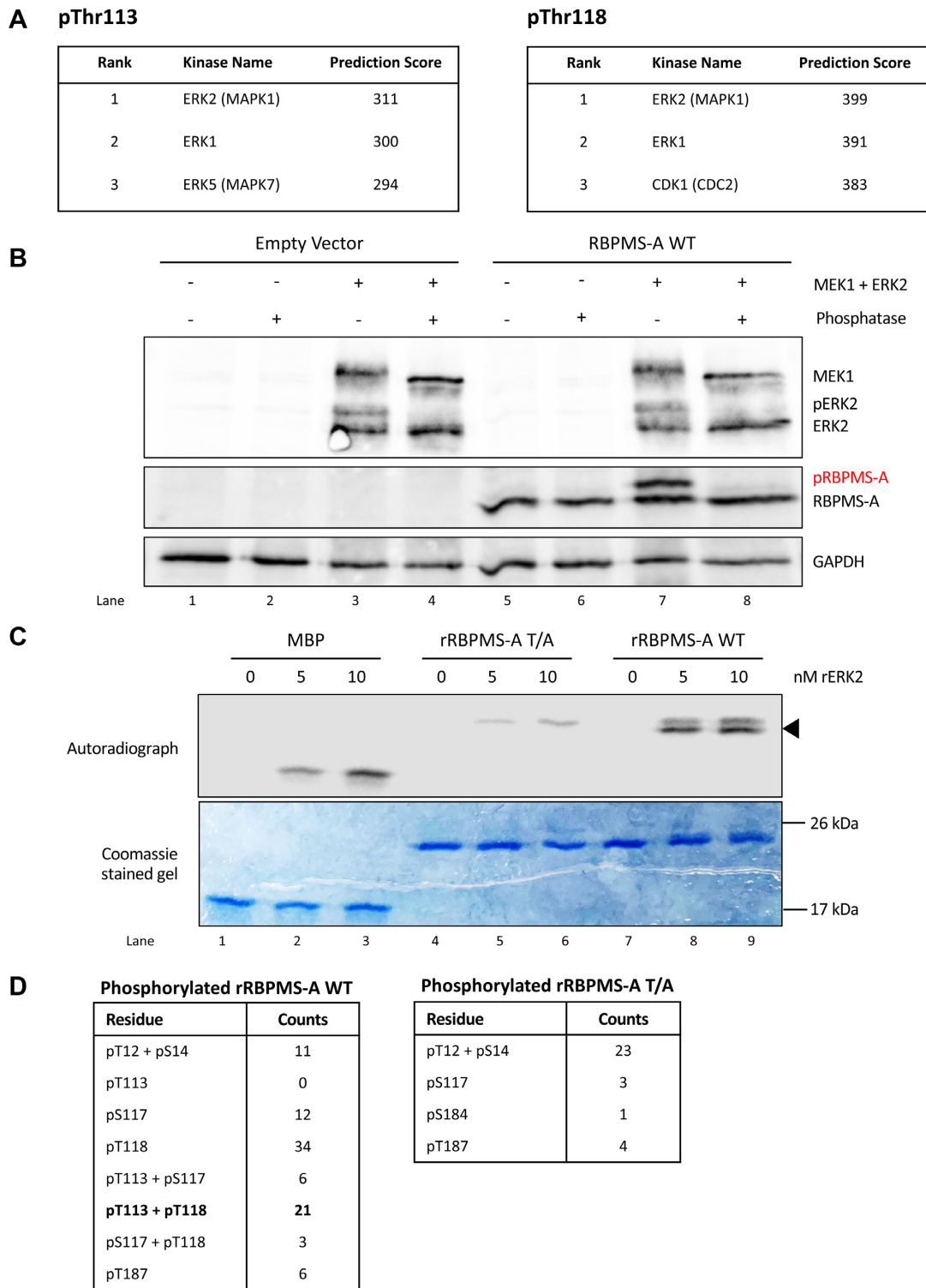


Figure 2. ERK2 phosphorylates RBPMS-A. (A) Top 3 predicted kinase scores for RBPMS-A phosphorylation at either Thr113 or Thr118 were obtained using Kinase Predictor V2 on PhosphoNET (www.phosphonet.ca). Scores were calculated accounting for the presence of neighboring phosphosites. Scores are not scaled to a maximum value. (B) Immunoblot of transiently transfected wild-type (WT) RBPMS-A with (+) or without (–) constitutively active (CA) MEK1 and wild-type ERK2. Following protein harvest, whole-cell lysates were treated (+) or mock-treated (–) with lambda phosphatase. Phosphorylated RBPMS-A (pRBPMS-A) is highlighted in red. Activated (phosphorylated) ERK2 (pERK2) can be seen in lanes 3 and 7. Immunoblot was probed with antibodies to FLAG and GAPDH. GAPDH was used as a loading control. (C) Recombinant wild-type (WT) RBPMS-A or RBPMS-A T/A were incubated with increasing nM amounts of highly active recombinant ERK2 in the presence of [γ - 32 P]ATP in an *in vitro* kinase assay. Proteins were stained with Coomassie blue (bottom) followed by autoradiography (top). Phosphorylation of RBPMS-A WT at T113 and T118 is indicated by the black arrow. Myelin basic protein (MBP) was used as a positive control. (D) Mass spectrometry results of *in vitro* kinase assay for either phosphorylated RBPMS-A WT or the T/A mutant. Phosphorylation sites of interest are bolded.

corresponds to phosphorylated RBPMS-A (Figure 2B, lane 8).

Next recombinant wild-type RBPMS-A was incubated *in vitro* with recombinant ERK2 and [γ - 32 P] ATP. Myelin basic protein (MBP), a known target of ERK2, was used as a positive control. RBPMS-A WT showed two radiolabeled bands (Figure 2C, upper panel, lanes 8 and 9) indicating that ERK2 can phosphorylate wild-type RBPMS-A at two or more positions. The RBPMS-A T/A showed only the fainter lower mobility band (lanes 5 and 6). The higher intensity lower bands (Figure 2C, arrow) are present only in the wild-type RBPMS-A lanes suggesting that these correspond to phosphorylation at T113 and/or T118. The upper bands present in the wild-type RBPMS-A lanes and RBPMS-A T/A lanes presumably correspond to phosphorylation of the protein at additional sites. Indeed, in addition to T113/118, both T12 and S144 also lie within X[pS/pT]P and PXxx[pS/pT]P consensus contexts for phosphorylation by ERK2 (33,34). Together, these results demonstrate that RBPMS-A is a substrate of ERK2.

Identification of RBPMS-A sites phosphorylated by ERK2

To directly determine which residues are phosphorylated by ERK2, we performed an *in vitro* kinase assay with unlabeled ATP, followed by mass spectrometry. The bands sent for analysis are shown in Supplementary Figure S2A. The results indicated that ERK2 phosphorylates RBPMS-A at Thr12, Ser14, Thr113, Ser117, Thr118 and Thr187 (Figure 2D), with the overwhelming majority of peptides corresponding either to single phosphorylation at Thr118 or dual phosphorylation at Thr113 and Thr118. Of note, phosphorylated Thr113 was only observed in conjunction with phospho-Thr118, suggesting that phosphorylation of Thr118 is necessary before phosphorylation occurs at Thr113, as previously reported (26,27).

Since Ser14 and Thr187 do not lie within a consensus context for ERK2 phosphorylation and their phosphorylation was observed at a lower frequency than Thr113 and 118, we concluded that these phosphorylation events might be due to the lower specificity of *in vitro* kinase assays so we did not consider them further (35). Although Ser144 has the sequence context for phosphorylation by ERK2, peptides containing S144 were not detected by mass spectrometry after various protease digestions, although subsequent experiments (below) indicated that S144 is phosphorylated by ERK2 in cells. Transfected phosphomimetic and non-phosphorylatable mutants at Thr12 and Ser144 (T12E, T12A, S144E, S144A, Figure 3A, B) and Ser 117 (S117E, Supplementary Figure S3) had identical splicing activity to WT RBPMS, indicating that phosphorylation at these residues plays no role in regulating RBPMS splicing activity. However, Thr12 and Ser144 and their adjacent prolines are conserved across vertebrates, suggesting that their phosphorylation may play some other role.

Cotransfection experiments using non-phosphorylatable mutants T113/118A (T/A), S144A and a combined triple mutant T/A + S144A, confirmed that these three residues are phosphorylated by ERK2 in HEK293T cells (Figure 3E). Two WT RBPMS bands were observed in the absence of MEK-CA and ERK2 (Figure 3E, lane 3) correspond-

ing to non-phosphorylated RBPMS (band 'A') and RBPMS basally phosphorylated at S144 (band 'B'). Upon addition of MEK-CA and ERK2 (lane 4), band A disappeared and a band corresponding to phosphorylation at T113/T118 and S144 appeared (band 'C'), with some residual band B. The identity of bands B and C was confirmed by the non-phosphorylatable mutants. The T/A mutant appeared identical to WT under resting conditions (lanes 3 and 5) but upon the addition of MEK-CA and ERK2, band B became more intense, and no band C was observed. With S144A, band B was not present, consistent with it corresponding to phosphorylation at S144 (lane 7). An additional band with mobility intermediate between A and B increased upon the addition of MEK1-CA and ERK2 (Figure 3E, lanes 7 and 8, band D), corresponding to phosphorylation at T113 and T118. For the triple mutant (T/A + S144A) bands B, C and D were completely abolished (Figure 3E, lane 10) consistent with their identification as RBPMS phosphorylated at S144, T113/T118/S144 and T113/T118 respectively.

Many kinases are recruited by specific docking sites located on their substrates. The motif 167-FTYP-170 on RBPMS (Figure 4A) is a perfect match to the ERK2 F-site docking motif FX(F/Y)P, and is located in a canonical position downstream of the phosphorylation sites (33,36–40). Consistent with its identification as an F-site, phosphorylation by ERK2 was substantially reduced for the F-site mutant compared to WT RBPMS (Figure 4B, lane 4 versus 2). The basal level of S144 phosphorylation of WT and T/A RBPMS-A was undisturbed by the F-site deletion (Figure 4B, lanes 3 and 7 compared to 1). However, deletion of the F-site reduced the level of ERK2 induced S144 phosphorylation in the T/A mutant (Figure 4B, lanes 6 and 8), while phosphorylation of Thr113 & Thr118 appears to be reduced by the removal of the F-site in the S144A mutant (Figure 4B, lanes 10 and 12). Together, these data suggest that the RBPMS-A F-site is important for ERK2 binding and phosphorylation of Thr113, 118 and Ser144. In contrast, F-site deletion had no effect on splicing activity (Supplementary Figure S4A–C), similar to the effect of deleting the region where T113 and T118 reside. Taken together, the preceding data indicate that ERK2 phosphorylates RBPMS at T113, T118 and S144, but that regulation of splicing activity results only from phosphorylation of RBPMS-A at both Thr113 and Thr118.

Phosphomimetic mutations directly impair RBPMS-A splicing activity

One way in which phosphorylation can influence splicing factor activity is by altering localization (41). To determine if the subcellular localization of RBPMS-A was affected by mutations in T113/118, FLAG-tagged RBPMS-A wild-type and the T/A and T/E mutants were transiently transfected in HEK293T cells and subcellular localization was analyzed by immunofluorescence microscopy. Both wild-type and T/A mutant RBPMS-A were localized primarily in the nucleus but excluded from nucleoli, with a minor fraction also evident in the cytoplasm around the nuclear periphery. In contrast, the T/E mutant was present in both the nucleus and the cytoplasm (Figure 5A). In an attempt to address whether the reduced splicing activity of the RBPMS-A

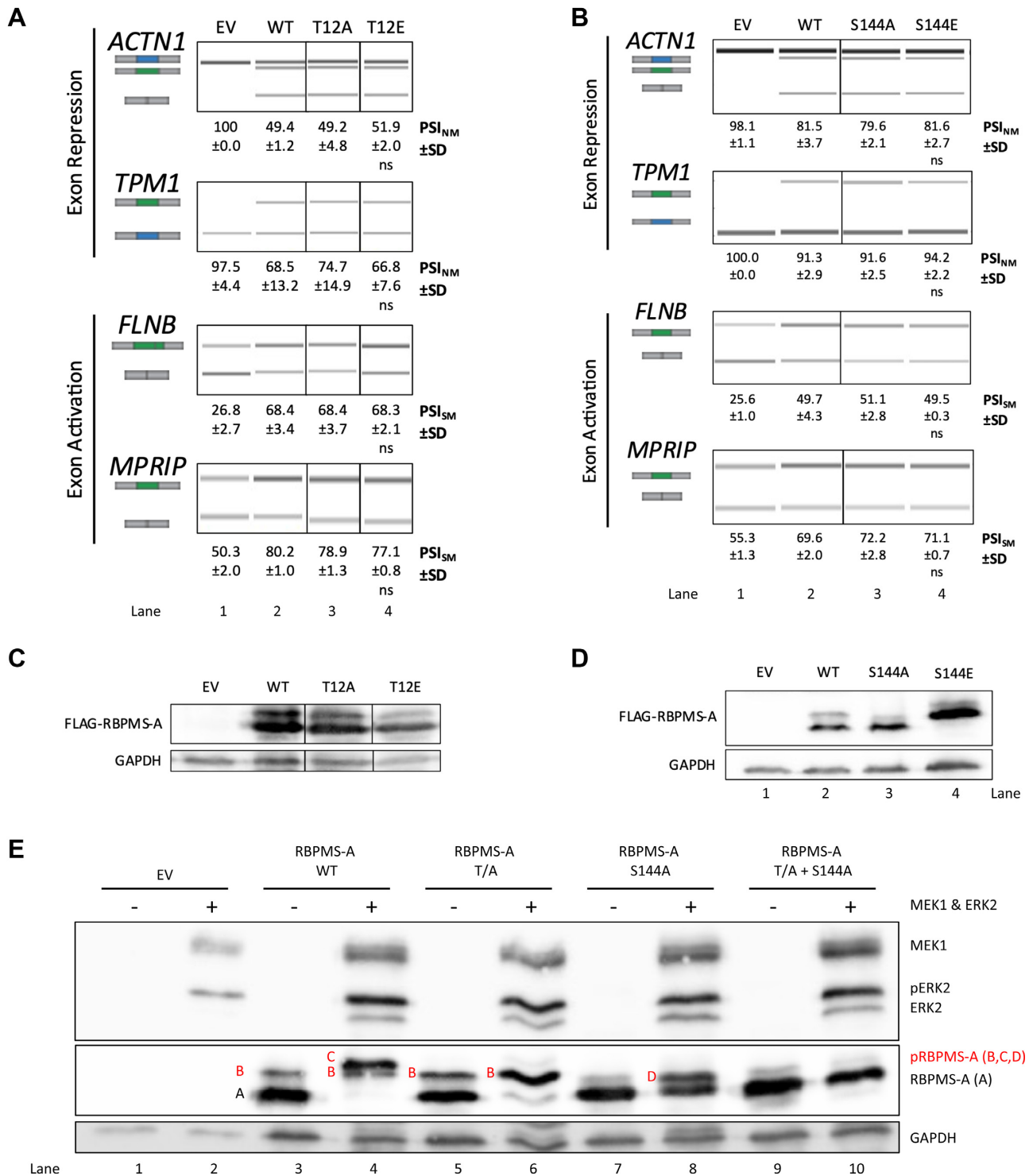


Figure 3. Other sites of phosphorylation identified on RBPMS-A have no effect on splicing. (A, B) Splicing analysis of the exon repression function of wild-type (WT) RBPMS-A and effectors in endogenous *ACTN1* and *TPM1*, and its exon activation function in endogenous *FLNB* and *MPRIP* in HEK293T cells. RT-PCR followed by visualization on QIAxcel. Cartoons below the gene names represent the PCR products. The blue exon in the cartoon represents the NM (non-smooth muscle) exon, while the green exon represents the SM (smooth muscle) exon. PSI (percent spliced in) values are the mean \pm SD ($n = 3$). A Student's *t*-test was used to determine statistical significance between wild-type RBPMS-A and effector. EV = empty vector. (C, D) Immunoblot of FLAG-RBPMS-A effectors used for splicing assays in (A, B). Whole-cell lysates were probed with antibodies to FLAG and GAPDH. GAPDH was used as a loading control. (E) Immunoblot of transiently transfected wild-type (WT) RBPMS-A and mutants with (+) or without (-) constitutively active (CA) MEK1 and wild-type ERK2. Phosphorylated RBPMS-A (pRBPMS-A) is highlighted in red. A = unphosphorylated RBPMS-A, B = pS144, C = pS144 + pT113 + pT118, D = pT113 + pT118. Activated (phosphorylated) ERK2 (pERK2) can be seen in lanes 2, 4, 6, 8 and 10. Immunoblot was probed with antibodies to FLAG and GAPDH. GAPDH was used as a loading control.

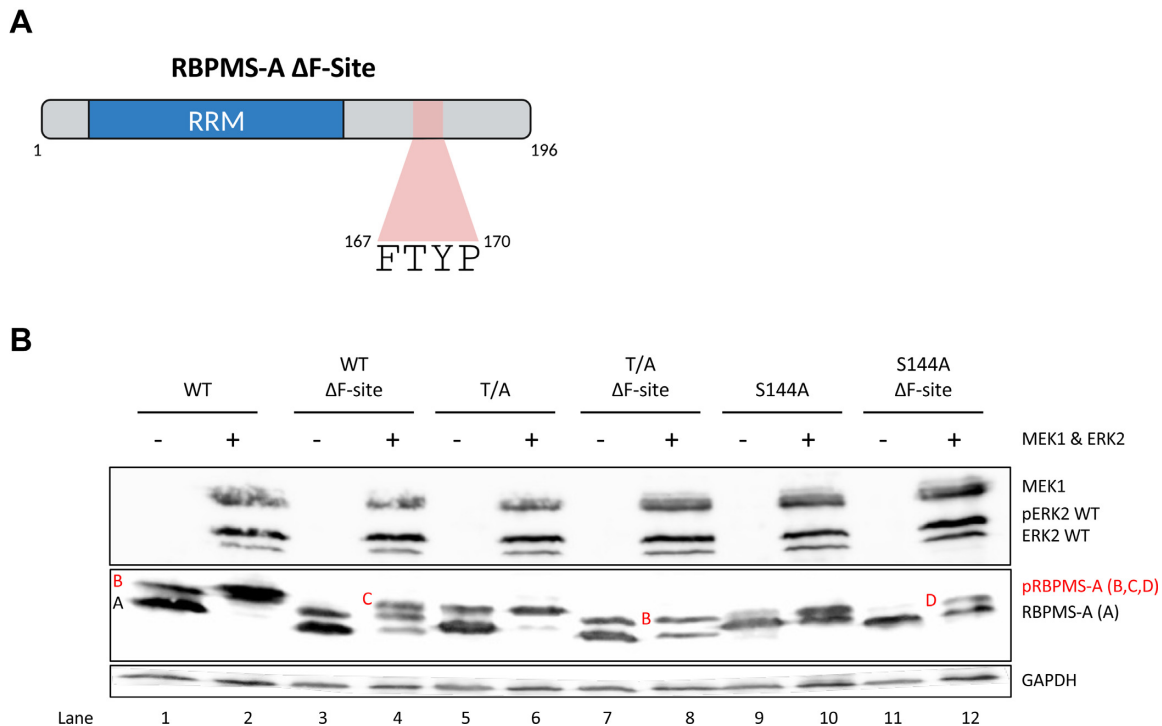


Figure 4. ERK2 phosphorylation of RBPMS-A depends upon an F-site. (A) Graphical representation of RBPMS-A Δ F-Site with the F-site region highlighted in red. The Δ F-Site mutation is the deletion of FTYP. Created with BioRender.com. (B) Immunoblot of transiently transfected wild-type (WT) RBPMS-A and mutants with (+) or without (–) constitutively active (CA) MEK1 and wild-type ERK2. Phosphorylated RBPMS-A (pRBPMs-A) is highlighted in red. A = unphosphorylated RBPMS-A, B = pS144, C = pS144 + pT113 + pT118, D = pT113 + pT118. Activated (phosphorylated) ERK2 (pERK2) can be seen in lanes 2, 4, 6, 8, 10 and 12. Immunoblot was probed with antibodies to FLAG and GAPDH. GAPDH was used as a loading control.

T/E mutant was due to its partial re-localization to the cytoplasm, we added an N-terminal exogenous nuclear localization signal (NLS) to each of the constructs (WT, T/A, T/E) and transiently transfected them into HEK293T cells to evaluate their splicing activity (Supplementary Figure S5A and B). Surprisingly, the exogenous NLS failed to rescue the partial cytoplasmic localization (Supplementary Figure S5D) of the RBPMS-A T/E mutant and also had no effect on splicing activity (Supplementary Figure S5A and B).

The immunofluorescence data indicated that only a fraction of the phosphomimetic T/E mutant is re-localized to the cytoplasm, which might not be sufficient to account for the loss of splicing regulation. To directly assess whether the phosphorylation of RBPMS-A directly affects its splicing activity, independent of localization, we expressed and purified recombinant RBPMS-A wild type, T/A and T/E (Supplementary Figure S6A). Previous work in the lab has shown that wild-type rBPMS-A represses (skips) exon 3 of a TM1-3-4 transcript in cell-free splicing assays, dependent on flanking CAC motifs (Yi Yang *et al.*, in preparation; Figure 5B). Therefore, using the well-characterized TM1-3-4 minigene (15,42), *in vitro* splicing assays were carried out with the recombinant RBPMS proteins to evaluate their splicing activity (Figure 5C). In the absence of added RBPMS, the 1–3–4 transcript primarily splices to include exon 3, indicated by some fully spliced 134 product as well as the prominent 1–34 partially spliced RNA (lanes 3 and 4). Upon addition of rBPMS-A WT, a switch in splicing was observed with dose-dependent decreases in exon 3 in-

clusion bands and a reciprocal increase in bands associated with exon skipping, the spliced 14 product, and the corresponding lariat that contains exon 3 as part of the intron (lanes 5–8 compared to lane 4). The rBPMS-A T/A mutant showed similar activity to WT (lanes 9–12 compared to lane 4), as in cell transfection assays. However, in agreement with our observations in HEK293T and PAC1 cells, the rBPMS-A T/E mutant showed near-complete loss of activity (lanes 13–16 compared to lane 4); at the highest concentration of T/E protein a slight increase in exon skipping products was observed, but exon 3 inclusion products were unaffected. These data demonstrate that the T113/118 phosphomimetic mutation directly reduces its splicing activity, suggesting that the loss of activity in cells (Figure 1B and E) is not merely localization-dependent.

Phosphomimetic mutation of RBPMS-A results in reduced RNA-binding affinity

To determine how the phosphorylation of RBPMS-A affects its splicing activity, we tested the effects of T113/118 mutations (T/E) upon RNA-binding. RBPMS dimers bind to tandem CAC motifs separated by a variable nucleotide spacer (5,43), and we have shown that RBPMS-A can bind to the three dual CAC motifs found in the intron upstream of *Tpm1* exon 3 (4). Therefore, we *in vitro* transcribed the intronic region upstream of *Tpm1* exon 3 (see Materials and Methods) for use in an electrophoretic mobility shift assay (EMSA) to examine the binding of rBPMS-A WT

and mutant proteins (Figure 6A). By estimating the concentration of protein at which 50% of RNA is bound we determined the apparent dissociation constants for comparison between the wild-type and mutants. The rBPMS-A T/E mutant has a higher apparent dissociation constant ($K_d = 756.1$ nM) compared to wild-type ($K_d = 212.9$ nM) and the T/A mutant ($K_d = 267.9$ nM) (Figure 6B). To further explore how phosphorylation affects RNA-binding, UV-crosslinking assays were carried out in the presence and absence of HeLa nuclear extract using the same *Tpm1* RNA (Figure 6C). Under both conditions, the RBPMS-A T/E mutant showed a significant reduction in crosslinking efficiency compared to WT. The reduction was more substantial in the presence of nuclear extract with only 7.8% crosslinked compared to WT (at 4 μ M; Figure 6C, upper panel). Thus, although the T/E mutant only had a 3-fold lower affinity for the *Tpm1* RNA (Figure 6A, B), in the presence of other RNA-binding proteins in nuclear extract the lower affinity leads to substantially lower RNA-binding. Taken together, these data suggest that phosphomimetic mutant (and by extension phosphorylation) of RBPMS-A inhibits RNA-binding, thereby explaining the loss of splicing regulatory activity.

Phosphomimetic mutant of RBPMS-A interferes with higher-order oligomerization and RNA contact

Recently, we have found that RBPMS-A undergoes higher-order oligomerization that is dependent upon the last 20 amino acids of the C-terminal intrinsically disordered region (IDR) of RBPMS-A. Truncation of this region impaired RBPMS-A oligomerization, multivalent RNA-binding, and splicing activity *in vitro* (Yi Yang *et al.*, in preparation). Therefore, we hypothesized that phosphorylation or phosphomimetic mutation of T113/118 might interfere with RNA-binding and activity by affecting oligomerization (and hence reducing the avidity of multivalent binding). An alternative, but not mutually exclusive, hypothesis is that the negatively charged phosphoT113/118 residues directly interfere with RNA-binding (via electrostatic effects) by the adjacent RRM. We decided to test both of these hypotheses. First, to investigate the potential effects upon multivalent RNA-binding, we used analytical ultracentrifugation (AUC) to analyze the sedimentation velocity (Figure 7A) and size distributions (Figure 7B) of wild-type rBPMS-A and the rBPMS-A T/A & T/E mutants. The WT and T/A mutant showed a mixture of dimers located at a sedimentation coefficient of $\sim 2.5S$ and higher-order oligomers located at a sedimentation coefficient of ~ 18 (Figure 7B), with a preponderance of the larger assemblies. Remarkably, the RBPMS-A T/E mutant showed a drastic decrease in the proportion of oligomers (Figure 7B, cyan line) when compared to the wild-type (maroon line) and the T/A mutant (purple line). However, the dimerization capability of the T/E mutant appears to remain intact as indicated by SEC-MALS (Supplementary Figure S7A and B). These data suggest that the phosphorylated RBPMS-A shows reduced oligomerization which ultimately may lead to lower activity by reduced multivalent avidity for RNA, as indicated by EMSA and UV-cross-linking.

Secondly, to explore whether phosphorylation at T113/118 might directly affect the ability of the RRM domain to interact with RNA, we used NMR spectroscopy to analyze truncated versions (amino acids 1–122) of rBPMS-A WT and T/E mutant, which were double-labeled with ^{13}C and ^{15}N (Figure 7C, Supplementary Figure S6B). Chemical shift assignment was carried out using published data for a related protein as a reference (RBPMS2, BMRB Entry 19298, (22)). The assignments were then extended to cover the disordered N- and C-terminal regions of RBPMS-A *ab initio*, facilitated by $^1H/^{13}C/^{15}N$ experiments at a reduced temperature that gave optimal peak intensities for these mobile regions (see Materials and Methods). Following assignment, chemical shift differences ($\Delta\delta$) between WT and T/E were quantified (Figure 7C) and linearly mapped from gray to red (greatest shift) onto a ribbon model of RBPMS-A bound to an RNA ligand (Figure 7D). The chemical shift differences were largest at or near the phosphomimetic mutations, as expected (Figure 7C). However, an inspection of the differences between the WT and T/E on the RRM domain itself revealed that a cluster of structurally contiguous residues in the RNA-binding site was strongly affected by the introduction of the phosphomimetic residues (Figure 7D), consistent with the predicted trajectory of the phosphomimetic tail (Supplementary Figure S8). Further, the RNA-binding face is lined with basic residues that would be expected to preferentially bind acidic residues and/or phosphothreonine (Figure 7E). These findings further support our hypothesis that RBPMS-A's RNA-binding region is directly affected by the addition of phosphomimetics (and by extension, phosphorylation) and that this effect likely reduces its RNA-binding affinity. Taken together, our data indicate that phosphorylation of RBPMS at T113/118 reduces RNA-binding by both directly interfering with the RNA-binding surface of the RRM domain and by reducing the avidity of multivalent RNA interaction due to the lower oligomerization state.

DISCUSSION

Cell-specific master splicing regulators have been defined by the following criteria: (i) they are required for cell-type specification or maintenance, (ii) their direct and indirect targets are functionally related and important for cell-type function, (iii) they are likely to regulate the activity of other splicing regulators, (iv) they have a wide dynamic range of activity, not limited by autoregulation and (v) they are regulated externally from the splicing network via transcriptional control or post-translational modifications (PTMs) (44). Previous work in our lab identified RBPMS as a smooth muscle master splicing regulator by addressing criteria 1–4 (4). Regarding criterion 5, it was already known that *RBPMS* transcription is switched off during smooth muscle dedifferentiation (4). Here, we provide evidence that the splicing regulatory activity of RBPMS protein is also directly down-regulated by phosphorylation, providing a rapid mechanism to switch off RBPMS activity as an early response during VSMC phenotypic modulation. A model summarizing our findings and their implications is shown in Figure 8. In differentiated contractile VSMCs (Figure

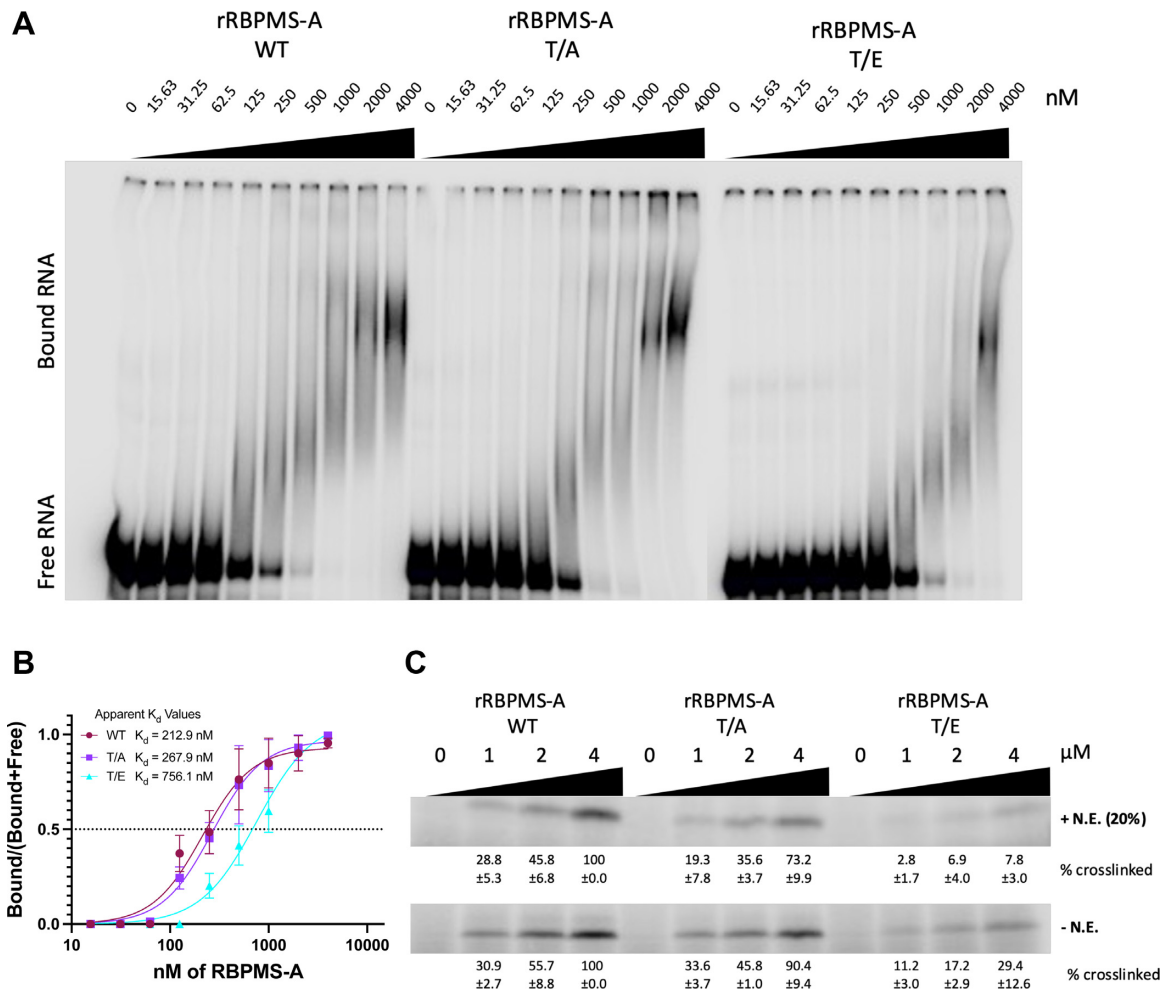


Figure 6. RBPMS-A phosphomimetic fails to bind to RNA. (A) Electrophoretic mobility shift assays (EMSAs) using recombinant wild-type (WT) RBPMS-A and the T/A and T/E mutants and an *in vitro* transcribed intron upstream of TPM1 exon 3. A decreasing serial dilution (1:10) of recombinant protein was used as indicated by the black triangles and the nM amounts listed above. Unbound or free RNA can be found at the bottom of the gel and the RBPMS + RNA complexes can be seen towards the upper right side of each gel. (B) Apparent K_d values were calculated by quantifying each lane in (A) as two fractions, ‘Bound’ (all complexes) and ‘Free’ and plotting $[\text{bound}]/[\text{bound} + \text{free}]$ against protein concentration; K_d was determined by the Hill equation. Quantification of measurements of wild-type RBPMS-A (WT; maroon circles) and mutants (T/A; purple squares & T/E; cyan triangles) binding to RNA from (A) were fitted to a Hill equation. The apparent dissociation constants (K_d) data points and error bars are from three technical replicates. Error bars are SEM. (C) UV-crosslinking using recombinant wild-type (WT) RBPMS-A, T/A, T/E mutants. *In vitro* crosslinking experiments were carried out in the presence (+N.E.) or absence (-N.E.) of 20% HeLa nuclear extract in a serial dilution (1:4; 4 to 1 μ M) as indicated by the black triangle with the μ M amounts listed above. % Cross-linked is normalized to 100% crosslinked at the highest concentration of WT (4 μ M) \pm SD.

8, left) non-phosphorylated RBPMS exists as dimers, mediated by the RRM domain (43), which are further assembled into larger oligomers, mediated by the C-terminal IDR. RBPMS oligomers can bind multivalently to target RNAs with multiple CAC motifs, such as *Tpm1* exon 3, to promote splicing patterns characteristic of differentiated VSMCs. Upon vascular injury or some other perturbation, activation of signaling pathways converges upon ERK1 or 2, which then phosphorylate RBPMS at Thr113 and 118 (Figure 8, center). Phosphorylation of T113/118 shifts the equilibrium from higher-order oligomers toward dimers, thereby reducing the avidity of multivalent RNA binding. In addition, the C-terminal region containing phospho-T113/118 acts as an RNA mimic, looping around and directly occluding the RNA binding surface of the RRM. Together, these two effects lead to reduced RNA binding by

RBPMS and switching of its regulated AS events to the splicing pattern characteristic of proliferative VSMCs (Figure 8, right). While all of our data are consistent with this model, some elements of the model will require further experimental investigation (discussed below).

Multiple lines of evidence indicate that Thr113/118 are phosphorylated and that ERK2 (and possibly ERK1) is the responsible kinase (Figures 2–4, Supplementary Figure S1). However, our conclusions about the functional consequences of phosphorylation rest upon the use of phosphomimetic glutamate mutations at T113 and T118. Potential concerns about this approach are first that the mutation might impair the normal function of the non-phosphorylated threonines. The retention of full RBPMS activity upon deletion of aa112–120 (Supplementary Figure S1C) strongly argues against this possibility, suggesting

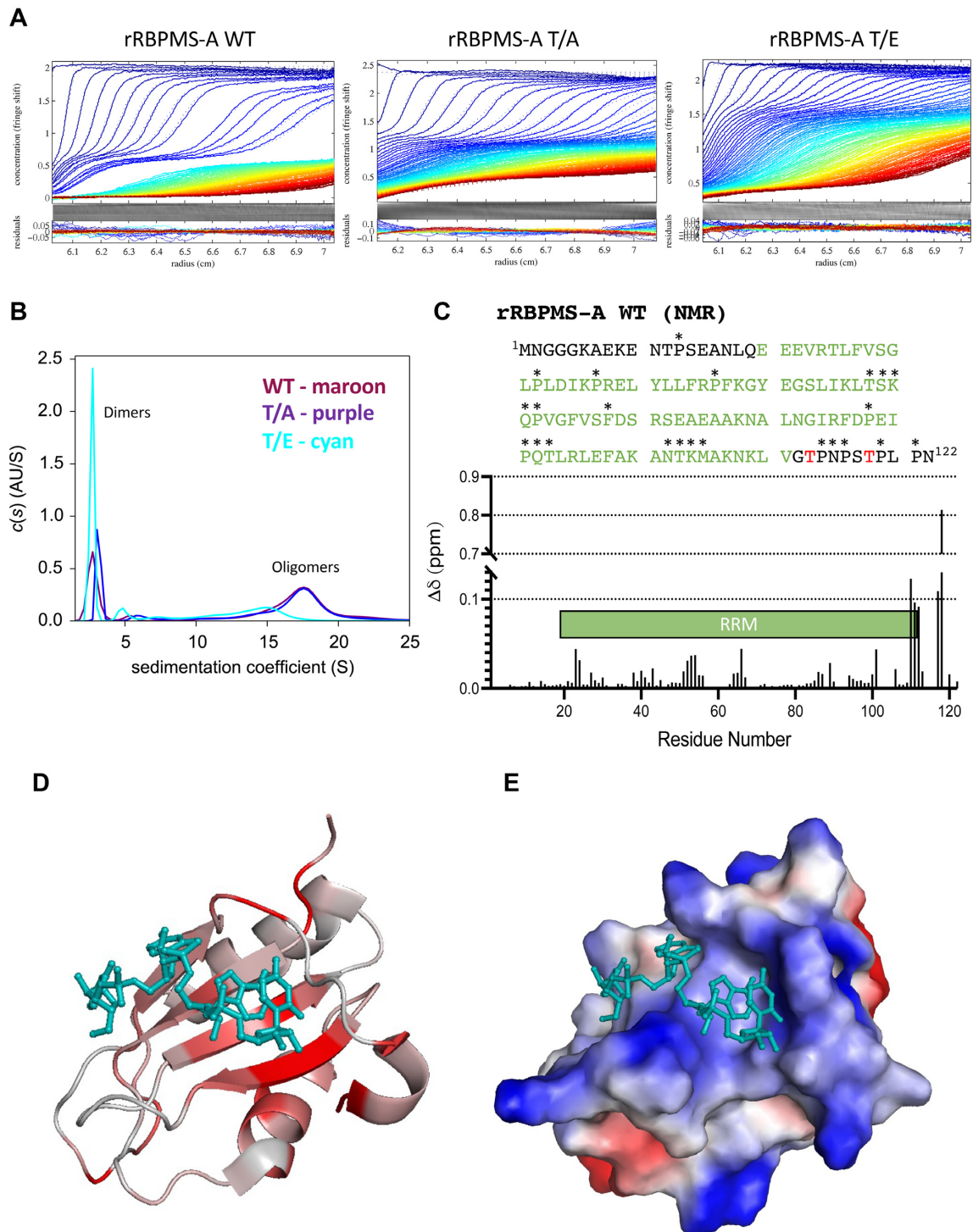


Figure 7. RBPMS-A phosphomimetic fails to oligomerize and directly affects its RNA binding site. (A) Analytical ultracentrifugation (AUC) sedimentation velocity acquired at 40 000 rpm for recombinant wild-type (WT) RBPMS-A and the T/A and T/E mutants at a concentration of 0.5 mg/ml. Radius (cm) is represented on the x-axis and the absorbance at 274 nm on the y-axis. Color temperature indicates the progress of time. (B) Size distribution profiles or continuous sedimentation coefficient distribution, $c(S)$, curves of each recombinant protein determined from their sedimentation velocity in (A). WT = maroon line, T/A = purple line, T/E = cyan. The peaks around a sedimentation coefficient of 2 represent the protein in a dimeric form while the peaks around 18 represent an oligomeric form. (C) RBPMS-A WT truncated amino acid sequence used for NMR, mutations at T113 and T118 (shown in red) to glutamic acid were used for the T/E mutant for NMR. The RRM is shown in green. Unlabeled residues are marked with asterisks (*). Quantified chemical shift differences between RBPMS-A WT and T/E are shown in the graph. Cartoon of the RRM domain is annotated in green. (D) Chemical shift differences mapped onto an RBPMS-A monomer. Ribbon model of RBPMS is colored according to $\Delta\delta$ on a scale of 0–0.01, linearly mapped from gray to red. The darkest red residues are the ones that have shifted the most. Bound RNA is shown for illustrative purposes (cyan). (E) The electrostatic potential of an RBPMS-A monomer bound to RNA (cyan) in the same orientation as (D), blue representing basic residues and red representing acidic residues.

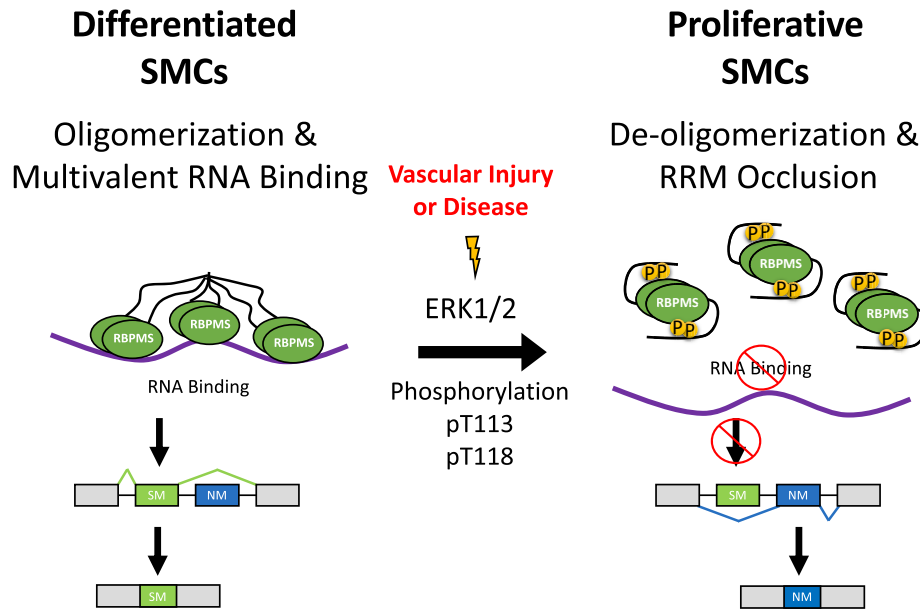


Figure 8. A model of splicing inactivation of RBPMS-A via phosphorylation. Vascular injury or disease activates ERK1/2 leading to the downstream phosphorylation of RBPMS-A at Thr113 and Thr118. Phosphorylation of RBPMS-A leads to de-oligomerization and RRM occlusion reducing RNA-binding and ultimately changing the splicing outcome, resulting in the increased inclusion of NM (non-smooth muscle) exons, found in the proliferative SMC cell type. In combination with the transcriptional downregulation of RBPMS, the rapid modulation of RBPMS via phosphorylation could play a vital role in phenotype plasticity during the vascular injury response and atherogenesis.

instead that this region serves only as a platform for regulatory input by phosphorylation. A second concern is that glutamate fails to completely mimic phospho-threonine. Glutamate residues have one negative charge at neutral pH, whereas phospho-threonine has between 1.5 and 2 negative charges. Phosphomimetic mutants are therefore likely to underestimate the consequences of phosphorylation, particularly where the phosphate group has a strong electrostatic effect. This is likely to be the case in the ‘RNA mimic’ mode of action where the RNA binding surface of the RRM is occluded by the phosphopeptide (Figure 7C–E, Supplementary Figure S8). While we do not yet understand the physical basis by which the phosphomimetics lead to de-oligomerization (Figure 7A and B), it seems likely that the T/E mutants underestimate the full consequences of phosphorylation, and that the down-regulation of RBPMS by phosphorylation might be more marked than we observe with phosphomimetic mutants. Consistent with this argument, we observed a complete loss of transfected RBPMS splicing activity upon co-transfection with MEK2-CA and ERK2 (data not shown), under conditions where RBPMS becomes fully phosphorylated (Figure 3E). However, the non-phosphorylatable T/A and T/A/S144A mutants were also inactive under these conditions, so the loss of activity could not be attributed to the phosphorylation of T113/118. A possible explanation is that ERK2 also phosphorylates and inactivates essential RBPMS coregulators such as RBFOX2 and ESRP2, which interact with RBPMS via its C-terminal IDR (Yang *et al.*, in preparation) and are known to be ERK targets. In this case, we would need non-phospho mutants not only of RBPMS but also of all the essential co-regulators, to bypass the inhibitory effect of ERK2. As an alternative, future *in vitro* studies to analyze

the effects of *bona fide* phosphorylation could use rRBPMS phosphorylated *in vitro*. However, a downside to this approach would be the heterogeneous and off-target phosphorylation that we observed with mass spectrometry (Figure 2D).

Phosphorylation of RNA binding proteins in general, and splicing factors in particular, have been widely documented. Phosphorylation can regulate RBP AS activity by affecting one or more of: RNA interactions; protein-protein interactions; subcellular localization; targeted degradation, reviewed in (45). In a limited number of cases, the consequences of phosphorylation are understood at a structural level (46). We observed some shift in localization of RBPMS T/E to the cytoplasm (Figure 5A, Supplementary Figure S5D), but the partial nature of this effect suggested that it was insufficient to have a major impact on nuclear RBPMS activity. Indeed, the loss of activity of RBPMS T/E in a cell-free splicing assay (Figure 5D) suggests that relocalization is unnecessary for the down-regulation of RBPMS splicing activity. Moreover, the reduced RNA binding of the phosphomimetic mutant (Figure 6) suggests that cytoplasmic RBPMS functions would also be down-regulated. This could be relevant for modulating the role of RBPMS as a translational regulator of lineage commitment in pluripotent cells by binding to 3' UTRs of target RNAs (47). Notably, multiple RBPMS bands were observed in ES cells, which likely arose both from the known RBPMS isoforms, but also the phospho-variants described here.

We uncovered two potential mechanisms, which are not mutually exclusive, that lead to reduced RNA binding and loss of RBPMS splicing regulation: direct occlusion of the RNA binding surface of the RRM (Figure 7C–E, Supplementary Figure S8), and reduced higher-order oligomeriza-

tion (i.e. homomeric protein-protein interactions) in favor of dimers. While RRM occlusion is likely to affect all RNA binding events, reduced oligomerization is likely to disproportionately affect events involving multivalent RNA binding (such as *Tpm1* exon 3), reminiscent of the differential effects of TDP-43 oligomerization mutations upon binding to long-multivalent regions compared to short multivalent sites (48). We have recently found that RBPMS oligomerization, which can progress to liquid-liquid phase separation, is mediated by the C-terminal IDR (Yang *et al.*, in preparation). A mutant with deletion of the C-terminal 20 amino acids unique to RBPMS-A lost splicing regulatory activity, oligomerization, interactions with other splicing co-regulators such as RBFOX2, ESRP2, RBM4, RBM14, RBM47 and binding to the multivalent *Tpm1* RNA substrate, similar to the phosphomimetic mutant (Figures 5–7). The phosphomimetic mutants showed differential loss of activity on different RNA substrates, generally having a greater impact on RBPMS repressed exons (Figure 1). It will be interesting in the future to investigate whether this is related to differential valency and distribution of binding sites around the different target exons, as observed for TDP43 mutants (48). An interesting possibility is that the two mechanisms that we have proposed for reduced RNA binding are actually physically coupled. In this scenario, the interaction of the phosphorylated T113/118 region with the RRM's RNA binding face would directly impact the ability of the C-terminal tail to engage in homomeric interactions leading to oligomerization, as well as potentially heteromeric interactions with other proteins. To pursue this question, we will first need to develop a better understanding of the 'molecular grammar' (49) underpinning RBPMS oligomerization and interactions with other proteins, and whether these hetero- and homo-typic interactions employ a common physical basis. The C-terminal tail of RBPMS contains a number of aromatic residues which could mediate oligomerization *via* pi-pi interactions with each other or *via* cation-pi interactions with three conserved C-terminal basic residues. We considered the possibility that electrostatic interactions between phospho threonines and basic residues might compete with cation-pi interactions leading to de-oligomerization. Arguing against this, mutation of the basic residues to alanine or isoleucine had no effect upon splicing regulatory activity (MDB and CWJS, unpublished observations). A recent report showed that RNA binding and splicing activity of the splicing regulator SAM68 is also downregulated by phosphorylation in its N and C-terminal IDRs, flanking the canonical RNA binding domain (50). However, in that case, the phosphorylation occurs directly within Arginine-Glycine regions antagonizing additional RNA that are necessary for stable binding.

During VSMC phenotypic switching, adhesion receptors, extracellular matrix, and growth factors relay extracellular signal inputs (2). Of all the growth factors that activate the Ras/Raf/MEK/ERK pathway, platelet-derived growth factor (PDGF) is considered to be the master growth factor driving vascular smooth muscle cell (VSMC) dedifferentiation (51). PDGF is released at the site of tissue damage and stimulates the migration and proliferation of VSMCs (52–55). Additionally, PDGF-stimulated migration of VSMCs to the intima, the inner layer of cells lining the arterial lu-

men, is an initial step in atherosclerosis (2). Upon activation of this signaling pathway, differentiated VSMCs transition to a more motile and proliferative state. We propose that an early step in this transition is the inactivation of the smooth muscle cell master splicing regulator, RBPMS. Inactivation of RBPMS via phosphorylation by ERK1/2 would provide SMCs with a rapid and reversible mechanism to precisely regulate the activity of this protein. RBPMS expression is not detected in dedifferentiated VSMCs in either cell culture (4) or *in vivo* following a carotid ligation injury (56), where RBPMS is present in contractile but absent in proliferative SMCs (A. Jacob and CWJS, unpublished observations). Testing whether RBPMS phosphorylation occurs at an early stage of the vascular injury response, and whether it plays a role in this response will be challenging. Given the small numbers of cells in an arterial lesion detection of RBPMS phosphorylated at T113/118 by western blot or mass spectrometry is not feasible. Detection by immunofluorescence might be possible, but would require antibodies specific for T113/118 phosphorylated RBPMS. However, following a carotid ligation injury, neointima formation involves a proliferative clonal outgrowth from a very small number of founder cells (56,57). If ERK-driven phosphorylation only occurs in those founder cells, it would be very difficult to detect even by immunofluorescence. An approach which might circumvent these problems would involve generation of a mouse line harboring the T113/118A mutations, which would be predicted to impair the early response to injury preceding turnover of RBPMS. Finally, in light of the fact that the potent transcriptional regulator necessary for SMC phenotypic transition, KLF4, is directly regulated by PDGF through activation of ERK1/2 (58–61), it is an attractive hypothesis that this pathway also regulates the master splicing regulator of SMCs, RBPMS. The regulation of transcription and splicing in concert would ensure the rapid onset of transition from a differentiated to proliferative phenotype.

Together, the data presented here support a model for the rapid modulation of the master SMC splicing regulator, RBPMS, via phosphorylation in response to external signals during the vascular injury response and atherogenesis. This results in RBPMS de-oligomerization and RRM occlusion, thereby reducing RNA-binding and ultimately changing the splicing outcome, working in concert with transcriptional regulation, when smooth muscle cells transition to a more motile and proliferative phenotype from their previously quiescent state (Figure 8).

DATA AVAILABILITY

The residues phosphorylated on RBPMS-A WT and T/A were identified via LC-MS/MS and mass spectrometry proteomics data have been deposited to the ProteomeXchange Consortium via the PRIDE (62) partner repository with the dataset identifier PXD034462. Residue assignments that were carried out following NMR were deposited in the Biological Magnetic Resonance Bank (BMRB) accession number 51654.

SUPPLEMENTARY DATA

Supplementary Data are available at NAR Online.

ACKNOWLEDGEMENTS

The authors would like to thank Matthew Watson, Department of Biochemistry, University of Cambridge, for NMR protein expression protocols, and Remkes Scheele, Department of Biochemistry, University of Cambridge, for providing purified active rERK2, and expression vectors for MEK1-CA and ERK2-WT. We thank Alex Borodavka and Giselle Lee for helpful comments and feedback on the manuscript. For the purpose of open access, the author has applied a Creative Commons Attribution (CC BY) license to any Author Accepted Manuscript version arising from this submission.

FUNDING

Wellcome Trust Investigator award [209368/Z/17/Z to C.W.J.S.]; United States Air Force (to M.D.B.); E.E.N.S. was supported by a studentship from the Conselho Nacional de Desenvolvimento Científico e Tecnológico [206813/2014-7]. Funding for open access charge: Cambridge Open Access Fund.

Conflict of interest statement. None declared.

REFERENCES

- World Health Organization (2019) In: *World Health Statistics: Monitoring Health for the SDGs, Sustainable Development Goals*. World Health Organization, Geneva.
- Frisantiene, A., Philippova, M., Erne, P. and Resink, T.J. (2018) Smooth muscle cell-driven vascular diseases and molecular mechanisms of VSMC plasticity. *Cell Signal*, **52**, 48–64.
- Owens, G.K., Kumar, M.S. and Wamhoff, B.R. (2004) Molecular regulation of vascular smooth muscle cell differentiation in development and disease. *Physiol. Rev.*, **84**, 767–801.
- Nakagaki-Silva, E.E., Gooding, C., Llorian, M., Jacob, A.G., Richards, F., Buckroyd, A., Sinha, S. and Smith, C.W. (2019) Identification of RBPMS as a mammalian smooth muscle master splicing regulator via proximity of its gene with super-enhancers. *Elife*, **8**, e46327.
- Farazi, T.A., Leonhardt, C.S., Mukherjee, N., Mihailovic, A., Li, S., Max, K.E.A., Meyer, C., Yamaji, M., Cekan, P., Jacobs, N.C. *et al.* (2014) Identification of the RNA recognition element of the RBPMS family of RNA-binding proteins and their transcriptome-wide mRNA targets. *RNA*, **20**, 1090–1102.
- Soufari, H. and MacKereth, C.D. (2017) Conserved binding of GCAC motifs by MEC-8, couch potato, and the RBPMS protein family. *RNA*, **23**, 308–316.
- Liu, L., Kryvokhyzha, D., Rippe, C., Jacob, A., Borreguero-Muñoz, A., Stenkula, K.G., Hansson-Ola, Christopher, Smith, W.J., Fisher, S.A. *et al.* (2022) Myocardin regulates exon usage in smooth muscle cells through induction of splicing regulatory factors. *Cell. Mol. Life Sci.*, **79**, 459.
- Deribe, Y.L., Pawson, T. and Dikic, I. (2010) Post-translational modifications in signal integration. *Nat. Struct. Mol. Biol.*, **17**, 666–672.
- Lovci, M.T., Bengtson, M.H. and Massier, K.B. (2016) Post-translational modifications and RNA-binding proteins. In: *Advances in Experimental Medicine and Biology*. Springer, New York LLC, Vol. **907**, pp. 297–317.
- Vu, N.T., Park, M.A., Shultz, J.C., Goehre, R.W., Hoferlin, L.A., Shultz, M.D., Smith, S.A., Lynch, K.W. and Chalfant, C.E. (2013) HnRNP U enhances caspase-9 splicing and is modulated by AKT-dependent phosphorylation of hnRNP L. *J. Biol. Chem.*, **288**, 8575–8584.
- Zhou, Z. and Fu, X.D. (2013) Regulation of splicing by SR proteins and SR protein-specific kinases. *Chromosoma*, **122**, 191–207.
- Rothman, A., Kulik, T.J., Taubman, M.B., Berk, B.C., Smith, C.W. and Nadal-Ginard, B. (1992) Development and characterization of a cloned rat pulmonary arterial smooth muscle cell line that maintains differentiated properties through multiple subcultures. *Circ.*, **86**, 1977–1986.
- Meerbrey, K.L., Hu, G., Kessler, J.D., Roarty, K., Li, M.Z., Fang, J.E., Herschkowitz, J.I., Burrows, A.E., Ciccia, A., Sun, T. *et al.* (2011) The pINDUCER lentiviral toolkit for inducible RNA interference in vitro and in vivo. *Proc. Natl. Acad. Sci. U.S.A.*, **108**, 3665–3670.
- Smith, C.W.J. and Nadal-Ginard, B. (1989) Mutually exclusive splicing of α -tropomyosin exons enforced by an unusual lariat branch point location: implications for constitutive splicing. *Cell*, **56**, 749–758.
- Gooding, C., Roberts, G.C. and Smith, C.W. (1998) Role of an inhibitory pyrimidine element and polypyrimidine tract binding protein in repression of a regulated alpha-tropomyosin exon. *RNA*, **4**, 85–100.
- Abmayr, S.M., Reed, R. and Maniatis, T. (1988) Identification of a functional mammalian spliceosome containing unspliced pre-mRNA. *Proc. Natl. Acad. Sci. U.S.A.*, **85**, 7216–7220.
- Schuck, P. (2000) Size-distribution analysis of macromolecules by sedimentation velocity ultracentrifugation and Lamm equation modeling. *Biophys. J.*, **78**, 1606–1619.
- Cavanagh, J., Skelton, N.J., Fairbrother, W.J., Rance, M. and Palmer, A.G.I. (2006) In: *Protein NMR Spectroscopy Principles and Practice*. 2nd edn. Academic Press.
- Panchal, S.C., Bhavesh, N.S. and Hosur, R.V. (2001) Improved 3D triple resonance experiments, HNN and HN(C)N, for HN and 15N sequential correlations in (13C, 15N) labeled proteins: application to unfolded proteins. *J. Biomol. NMR*, **20**, 135–147.
- Hyberts, S.G., Takeuchi, K. and Wagner, G. (2010) Poisson-gap sampling and forward maximum entropy reconstruction for enhancing the resolution and sensitivity of protein NMR data. *J. Am. Chem. Soc.*, **132**, 2145–2147.
- Bostock, M.J., Holland, D.J. and Nietlisbach, D. (2012) Compressed sensing reconstruction of undersampled 3D NOESY spectra: application to large membrane proteins. *J. Biomol. NMR*, **54**, 15–32.
- Sagnol, S., Yang, Y., Bessin, Y., Allemand, F., Hapkova, I., Notarnicola, C., Guichou, J.F., Faure, S., Labesse, G. and de Santa Barbara, P. (2014) Homodimerization of RBPMS2 through a new RRM-interaction motif is necessary to control smooth muscle plasticity. *Nucleic Acids Res.*, **42**, 10173–10184.
- Vranken, W.F., Boucher, W., Stevens, T.J., Fogh, R.H., Pajon, A., Llinas, M., Ulrich, E.L., Markley, J.L., Ionides, J. and Laue, E.D. (2005) The CCPN data model for NMR spectroscopy: development of a software pipeline. *Proteins: Struct. Funct. Genet.*, **59**, 687–696.
- Zuiderweg, E. (2002) Mapping protein–protein interactions in solution by NMR spectroscopy. *Biochemistry*, **41**, 1–7.
- Hornbeck, P.V., Zhang, B., Murray, B., Kornhauser, J.M., Latham, V. and Skrzypek, E. (2015) PhosphoSitePlus, 2014: mutations, PTMs and recalibrations. *Nucleic Acids Res.*, **43**, D512–D520.
- Dephoure, N., Zhou, C., Villén, J., Beausoleil, S.A., Bakalarski, C.E., Elledge, S.J. and Gygi, S.P. (2008) A quantitative atlas of mitotic phosphorylation. *Proc. Natl. Acad. Sci. U.S.A.*, **105**, 10762–10767.
- Kettenbach, A.N., Schweppe, D.K., Faherty, B.K., Pechenick, D., Pletnev, A.A. and Gerber, S.A. (2011) Quantitative phosphoproteomics identifies substrates and functional modules of aurora and Polo-like kinase activities in mitotic cells. *Sci. Signal*, **4**, rs5.
- Sharma, K., D'Souza, R.C.J., Tyanova, S., Schaab, C., Wiśniewski, J.R., Cox, J. and Mann, M. (2014) Ultradeep human phosphoproteome reveals a distinct regulatory nature of Tyr and Ser/Thr-Based signaling. *Cell Rep.*, **8**, 1583–1594.
- Mertins, P., Mani, D.R., Ruggles, K.v., Gillette, M.A., Clauser, K.R., Wang, P., Wang, X., Qiao, J.W., Cao, S., Petralia, F. *et al.* (2016) Proteogenomics connects somatic mutations to signalling in breast cancer. *Nature*, **534**, 55–62.
- Ochoa, D., Jarnuczak, A.F., Gehre, M., Soucheray, M., Kleefeldt, A.A., Veitez, C., Hill, A., Garcia-Alonso, L., Swaney, D.L., Vizcaino, J.A.A. *et al.* (2019) The functional landscape of the human phosphoproteome. *Nat. Biotechnol.*, **38**, 365–373.
- Carlson, S.M., Chouinard, C.R., Labadorf, A., Lam, C.J., Schmelzle, K., Fraenkel, E. and White, F.M. (2011) Large-scale discovery of ERK2 substrates identifies ERK-mediated transcriptional regulation by ETV3. *Sci. Signal*, **4**, 11.
- Lee, C.R., Park, Y.H., Kim, Y.R., Peterkofsky, A. and Seok, Y.J. (2013) Phosphorylation-dependent mobility shift of proteins on SDS-PAGE

- is due to decreased binding of SDS. *Bull. Korean Chem. Soc.*, **34**, 2063–2066.
33. Roskoski, R. (2012) ERK1/2 MAP kinases: structure, function, and regulation. *Pharmacol. Res.*, **66**, 105–143.
 34. Davis, R.J. (1993) The mitogen-activated protein kinase signal transduction pathway. *J. Biol. Chem.*, **268**, 14553–14556.
 35. Xue, L. and Tao, W.A. (2013) Current technologies to identify protein kinase substrates in high throughput. *Front. Biol. (Beijing)*, **8**, 216.
 36. Bermudez, O., Pagès, G. and Gimond, C. (2010) The dual-specificity MAP kinase phosphatases: critical roles in development and cancer. *Am. J. Physiol. Cell Physiol.*, **299**, C189–C202.
 37. Tanoue, T., Adachi, M., Moriguchi, T. and Nishida, E. (2000) A conserved docking motif in MAP kinases common to substrates, activators and regulators. *Nat. Cell Biol.*, **2**, 110–116.
 38. Jacobs, D., Glossip, D., Xing, H., Muslin, A.J. and Kornfeld, K. (1999) Multiple docking sites on substrate proteins form a modular system that mediates recognition by ERK MAP kinase. *Genes Dev.*, **13**, 163–175.
 39. Sharrocks, A.D., Yang, S.H. and Galanis, A. (2000) Docking domains and substrate-specificity determination for MAP kinases. *Trends Biochem. Sci.*, **25**, 448–453.
 40. Sheridan, D.L., Kong, Y., Parker, S.A., Dalby, K.N. and Turk, B.E. (2008) Substrate discrimination among mitogen-activated protein kinases through distinct docking sequence motifs. *J. Biol. Chem.*, **283**, 19511–19520.
 41. Misteli, T., Cáceres, J.F., Clement, J.Q., Krainer, A.R., Wilkinson, M.F. and Spector, D.L. (1998) Serine phosphorylation of SR proteins is required for their recruitment to sites of transcription in vivo. *J. Cell Biol.*, **143**, 297–307.
 42. Wollerton, M.C., Gooding, C., Robinson, F., Brown, E.C., Jackson, R.J. and Smith, C.W.J. (2001) Differential alternative splicing activity of isoforms of polypyrimidine tract binding protein (PTB). *RNA*, **7**, 819–832.
 43. Teplova, M., Farazi, T.A., Tuschl, T. and Patel, D.J. (2016) Structural basis underlying CAC RNA recognition by the RRM domain of dimeric RNA-binding protein RBPMS. *Q. Rev. Biophys.*, **49**, e1.
 44. Jangi, M. and Sharp, P.A. (2014) Building robust transcriptomes with master splicing factors. *Cell*, **159**, 487–498.
 45. Stamm, S. (2008) Regulation of alternative splicing by reversible protein phosphorylation. *J. Biol. Chem.*, **283**, 1223–1227.
 46. Thapar, R. (2015) Structural basis for regulation of RNA-binding proteins by phosphorylation. *ACS Chem. Biol.*, **10**, 652.
 47. Bartsch, D., Kalamkar, K., Ahuja, G., Bazzi, H., Papantonis, A. and Kurian, L. (2021) Translational specialization in pluripotency by RBPMS poises future lineage-decisions. bioRxiv doi: <https://doi.org/10.1101/2021.04.12.439420>, 12 April 2021, preprint: not peer reviewed.
 48. Hallegger, M., Chakrabarti, A.M., Lee, F.C.Y., Lee, B.L., Amalietti, A.G., Odeh, H.M., Copley, K.E., Rubien, J.D., Portz, B., Kuret, K. *et al.* (2021) TDP-43 condensation properties specify its RNA-binding and regulatory repertoire. *Cell*, **184**, 4680–4696.
 49. Wang, J., Choi, J.M., Holehouse, A.S., Lee, H.O., Zhang, X., Jahnel, M., Maharana, S., Lemaitre, R., Pozniakovskiy, A., Drechsel, D. *et al.* (2018) A molecular grammar governing the driving forces for phase separation of Prion-like RNA binding proteins. *Cell*, **174**, 688–699.
 50. Malki, I., Liepina, I., Kogelnik, N., Lightfoot, A., Gonchar, O., Watmuff, H., Bottrill, A., Fry, A.M. and Dominguez, C. (2022) Cdk1-mediated threonine phosphorylation of sam68 modulates its RNA binding, alternative splicing activity, and cellular functions. bioRxiv doi: <https://doi.org/10.1101/2022.03.23.485498>, 23 March 2022, preprint: not peer reviewed.
 51. Mack, C.P. (2011) Signaling mechanisms that regulate smooth muscle cell differentiation. *Arterioscler. Thromb. Vasc. Biol.*, **31**, 1495–1505.
 52. Kohler, N. and Lipton, A. (1974) Platelets as a source of fibroblast growth-promoting activity. *Exp. Cell Res.*, **87**, 297–301.
 53. Ross, R., Glomset, J., Kariya, B. and Harker, L. (1974) A platelet dependent serum factor that stimulates the proliferation of arterial smooth muscle cells in vitro. *Proc. Natl. Acad. Sci. U.S.A.*, **71**, 1207–1210.
 54. Grotendorst, G.R., Chang, T., Seppä, H.E.J., Kleinman, H.K. and Martin, G.R. (1982) Platelet-derived growth factor is a chemoattractant for vascular smooth muscle cells. *J. Cell. Physiol.*, **113**, 261–266.
 55. Marx, G., Korner, G., Mou, X. and Gorodetsky, R. (1993) Packaging zinc, fibrinogen, and factor XIII in platelet alpha-granules. *J. Cell. Physiol.*, **156**, 437–442.
 56. Chappell, J., Harman, J.L., Narasimhan, V.M., Yu, H., Foote, K., Simons, B.D., Bennett, M.R. and Jørgensen, H.F. (2016) Extensive proliferation of a subset of differentiated, yet plastic, medial vascular smooth muscle cells contributes to neointimal formation in mouse injury and atherosclerosis models. *Circ. Res.*, **119**, 1313–1323.
 57. Dobnikar, L., Taylor, A.L., Chappell, J., Oldach, P., Harman, J.L., Oerton, E., Dzierzak, E., Bennett, M.R., Spivakov, M. and Jørgensen, H.F. (2018) Disease-relevant transcriptional signatures identified in individual smooth muscle cells from healthy mouse vessels. *Nat. Commun.*, **9**, 4567.
 58. Deaton, R.A., Gan, Q. and Owens, G.K. (2009) Sp1-dependent activation of KLF4 is required for PDGF-BB-induced phenotypic modulation of smooth muscle. *Am. J. Physiol.-Heart Circ. Physiol.*, **296**, H1027–H1037.
 59. Shankman, L.S., Gomez, D., Cherepanova, O.A., Salmon, M., Alencar, G.F., Haskins, R.M., Swiatlowska, P., Newman, A.A.C., Greene, E.S., Straub, A.C. *et al.* (2015) KLF4-dependent phenotypic modulation of smooth muscle cells has a key role in atherosclerotic plaque pathogenesis. *Nat. Med.*, **21**, 628–637.
 60. Salmon, M., Gomez, D., Greene, E., Shankman, L. and Owens, G.K. (2012) Cooperative binding of KLF4, pELK-1, and HDAC2 to a G/C repressor element in the SM22 α promoter mediates transcriptional silencing during SMC phenotypic switching in vivo. *Circ. Res.*, **111**, 685–696.
 61. Kim, M.O., Kim, S.H., Cho, Y.Y., Nadas, J., Jeong, C.H., Yao, K., Kim, D.J., Yu, D.H., Keum, Y.S., Lee, K.Y. *et al.* (2012) ERK1 and ERK2 regulate embryonic stem cell self-renewal through phosphorylation of klf4. *Nat. Struct. Mol. Biol.*, **19**, 283–290.
 62. Perez-Riverol, Y., Bai, J., Bandla, C., Garcia-Seisdedos, D., Hewapathirana, S., Kamatchinathan, S., Kundu, D.J., Prakash, A., Frericks-Zipper, A., Eisenacher, M. *et al.* (2022) The PRIDE database resources in 2022: a hub for mass spectrometry-based proteomics evidences. *Nucleic Acids Res.*, **50**, D543–D552.